Journal of Inorganic Biochemistry 199 (2019) 110789

Contents lists available at ScienceDirect

Journal of Inorganic Biochemistry

journal homepage: www.elsevier.com/locate/jinorgbio

Structural characterization and biological properties of silver(I) tris (pyrazolyl)methane sulfonate

Joana Almeida[a], Catarina Roma-Rodrigues[a], Abdallah G. Mahmoud[b], M. Fátima C. Guedes da Silva[b], Armando J.L. Pombeiro[b], Luísa M.D.R.S. Martins[b], Pedro V. Baptista[a], Alexandra R. Fernandes[a,b,*]

[a] UCIBIO, Departamento Ciências da Vida, Faculdade de Ciências e Tecnologia, Universidade Nova de Lisboa, Campus Caparica, 2829-516 Caparica, Portugal
[b] Centro de Química Estrutural, Instituto Superior Técnico, Universidade de Lisboa, Av. Rovisco Pais, 1049-001 Lisboa, Portugal

ARTICLE INFO

Dedicated to Prof. Debbie Crans as a recognition of her distinguished contributions for the advancement of Inorganic and Bioinorganic Chemistries.

Keywords:
Ovarian carcinoma
Antiproliferative activity
Silver complexes
Cell death
2-D electrophoresis

ABSTRACT

The water-soluble 1D helical coordination polymer $[Ag(Tpms)]_n$ (**1**) [Tpms = tris(pyrazolyl)methane sulfonate, $^{-}O_3SC(pz)_3$; pz = pyrazolyl] was synthesized and fully characterized, its single-crystal X-ray diffraction analysis revealing the ligand acting as a bridging chelate N_3-donor ligand. The antiproliferative potential of **1** was performed on two human tumour cell lines, A2780 and HCT116, and in normal fibroblasts, with a much higher effect in the former cell line (IC_{50} of 0.04 μM) as compared to the latter cell line and to normal fibroblasts. Compound **1** does not alter cell cycle progression but interferes with the adherence of A2780 cells triggering cell apoptosis. Apoptosis appears to occur via the extrinsic pathway (no changes in mitochondria membrane potential, reactive oxygen species (ROS) and pro-apoptotic (B-cell lymphoma 2 (BCL-2) associated protein (BAX))/anti-apoptotic (BCL-2) ratio) being this hypothesis also supported by the presence of silver mainly in the supernatants of A2780 cells. Results also indicated that cell death via autophagy was triggered. Proteomic analysis allowed us to confirm that compound **1** is able to induce a stress response in A2780 cells that is related with its antiproliferative activity and the trigger of apoptosis.

1. Introduction

Cancer includes a large group of diseases characterized by the rapid division of abnormal cells beyond their usual boundaries that can invade adjacent tissues and/or spread to distant organs. [1,2] According to the World Health Organization (WHO), cancer is the second leading cause of death globally and is estimated that 9.6 million people died due to this disease in 2018. [3] Chemotherapy has shown to be highly effective in the treatment of cancer but most of chemotherapeutic agents applied today in the clinical practice present two major drawbacks: the development of toxicity in healthy tissues and the emergence of intrinsic and acquired (multi)drug resistance [1,4]. Since the discovery of the anticancer activity of cisplatin, [5] several metal complexes have been synthesized and explored regarding their potential in inhibiting cancer cell proliferation without promoting the undesirable side effects that limit the efficacy of chemotherapy [6,7]. Metal complexes are versatile molecules due to the intrinsic characteristics of both metal centers and ligands, providing for a wide range of reactional properties such as redox activity, variable coordination modes and reactivity toward the organic substrate [8]. Silver complexes have been used for a long time in the treatment of infected wounds and burn cases and in the coatings of medical devices due to their antimicrobial properties [7,9]. The antimicrobial and potentially the antitumor properties of silver complexes are due to its peculiar mechanism of action. Indeed, although the pathways of action have not been fully elucidated, the antimicrobial action of silver can be exerted in several ways: i) permeabilization of the cell by binding to essential membrane enzymes or by destruction of cell wall integrity due to the removal of electrons of this component; (ii) changes in cellular metabolism through interaction with enzymes, protein denaturation, inhibition of bacterial respiration or oxidation of ATP; (iii) induction of reactive oxygen species (ROS). Thus, in principle, the mechanisms of action of silver complexes on tumour cells may be similar. According to Medici et al. [10] silver anticancer action is based on different mechanisms compared to those of platinum derivatives, in terms DNA interaction, mitochondrial membrane targeting, and inhibition of thioredoxin

* Corresponding author at: UCIBIO, Departamento Ciências da Vida, Faculdade de Ciências e Tecnologia, Universidade Nova de Lisboa, Campus Caparica, 2829-516 Caparica, Portugal.
E-mail address: ma.fernandes@fct.unl.pt (A.R. Fernandes).

https://doi.org/10.1016/j.jinorgbio.2019.110789
Received 22 May 2019; Received in revised form 18 July 2019; Accepted 19 July 2019
Available online 19 July 2019
0162-0134/

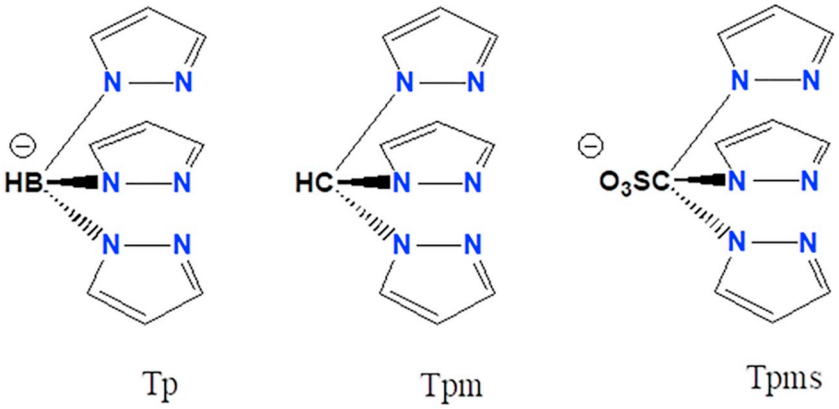

Chart 1. Chemical structures of anion (Tp), tris(pyrazolyl)methane (Tpm) and tris(pyrazolyl)methane sulfonates (Tpms).

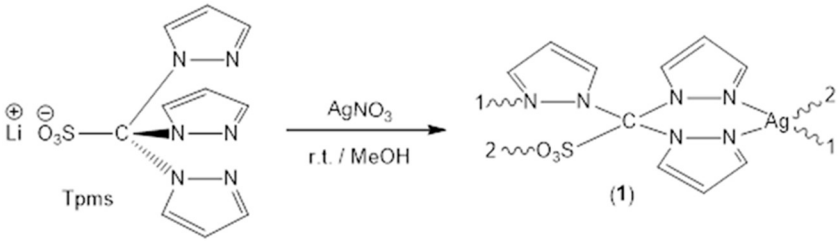

Scheme 1. Synthesis of compound **1**.

reductase, leading to mitochondria-derived apoptosis, similarly to what has been observed with gold complexes. Recently, cytotoxic properties of silver(I) complexes have attracted great interest, because some of them exhibit a higher cytotoxic activity when compared to cisplatin with relatively low toxicity in normal cells (selectivity toward cancer cells) [11]. The activity of silver complexes is strictly connected with their water solubility and stability, lipophilicity, redox ability and rate of release of the silver ions. These properties are strongly conditioned by the ligand [10,11]. In 1966, Trofimenko introduced the tris(pyrazolyl)borate anion (Tp) as ligand (Chart 1), [12] which, along with subsequent derivatives including tris(pyrazolyl)methane (tpm) analogues, [13] rapidly occupied a prominent position in coordination chemistry in view of their ability to behave as versatile nitrogen chelating species. The coordination flexibility of these ligands, resulting from steric and electronic modifications in their structure, highly influences the stability, inertia and reactivity of the derived metal complexes [14]. The flexible anionic assembly tris(pyrazolyl)methane sulfonate (Tpms) (Chart 1) was later synthesized by Klaui and co-workers, [15] where the methane sulfonate group instead of a BH provided the anion with a high stability toward hydrolysis, high solubility in polar solvents and structure robustness over a wide pH range in aqueous solution [13–15]. In addition, Tpms has the advantage of coordination in a tridentate or bidentate way, [16] in the former case working as a *NNN*- or *NNO*-donor, and in the latter as a *NN*- or *NO*-donor [17]. Metal complexes containing the ligands Tp, Tpm and Tpms have being shown promising chemotherapeutic agents [18]. Complexes with copper(I), Tp and other ligands showed improved selectivity toward tumour cells relative to normal cells. [19] A manganese complex, $[Mn(CO)_3(tpm)]$ PF6, exhibited improved toxicity in HT29 human cells photodynamic therapy, relative to the currently clinically used 5-fluorouracil [20]. Cobalt complexed with Tpm presented lower IC_{50} values in human colorectal adenocarcinoma, HCT116, and human hepatocarcinoma, HepG2, cell lines than common antitumor drugs cisplatin and doxorubicin [21]. Tpms were also analysed when coordinated with Ag(I), with or without other ligands, in A375 human malignant melanoma cell lines [22]. Interestingly, a direct correlation between cytotoxic effect and DNA binding constants of the complexes, with [Ag(Tpms)] showing higher cytotoxicity than $AgNO_3$ [22].

The present study aimed to evaluate the antiproliferative potential of the coordination polymer $[Ag(Tpms)]_n$ (**1**) providing insights into the mechanisms of its biological activity, namely cell death pathway, cell cycle effect, ROS generation and changes in protein expression through a comparative proteomic analysis.

2. Results and discussion

The reaction of the lithium salt of Tpms with $AgNO_3$ in methanol at room temperature leads to the coordination polymer $[Ag(Tpms)]_n$ (**1**) in good yield (Scheme 1).

The formulation of compound **1** was confirmed by spectroscopic and analytical data (see experimental section) and its structure was established by single crystal X-ray diffraction (SCXRD). Both the ^1H and ^{13}C NMR spectra of the compound display a set of resonances, one for each type of proton or carbon, similar to those of Tpms in the starting material (Fig. 1; see also Figs. S1-S5 in Supplementary Material file) although downfield shifted due to coordination to the metal centre. Compound **1** shows a good solubility in water, dimethyl sulfoxide (DMSO) and acetonitrile (MeCN). It is stable in air in the solid state, but in all solutions and within ca. four days a black solid of silver oxide is formed.

2.1. X-ray crystal structure

The molecular structure of compound **1** was established by SCXRD analysis (Fig. 2).

It crystallized in the monoclinic space group *P 21/c*, the asymmetric unit comprising two Tpms anions and two silver cations. Upon symmetry expansion, a 1D polymeric chain is revealed, spreading along the crystallographic *b* axis. Each Tpms unit bridges two metal centres acting as a *NN*-donor to one Ag(I) and as a *NO*-donor to another (Fig. 2), forming a 1D helical coordination polymer with the sulfonate groups alternating their positions along the infinite Ag··· Ag chain (Fig. 3). The metal centre exhibits N_3O-square planar geometry with Ag—N lengths in the 2.138(7) 2.453(7) Å range, and far-off bond interactions involving the silver cations and the $O_{sulfonate}$ atoms [Ag1-O4 of 2.915(6) and

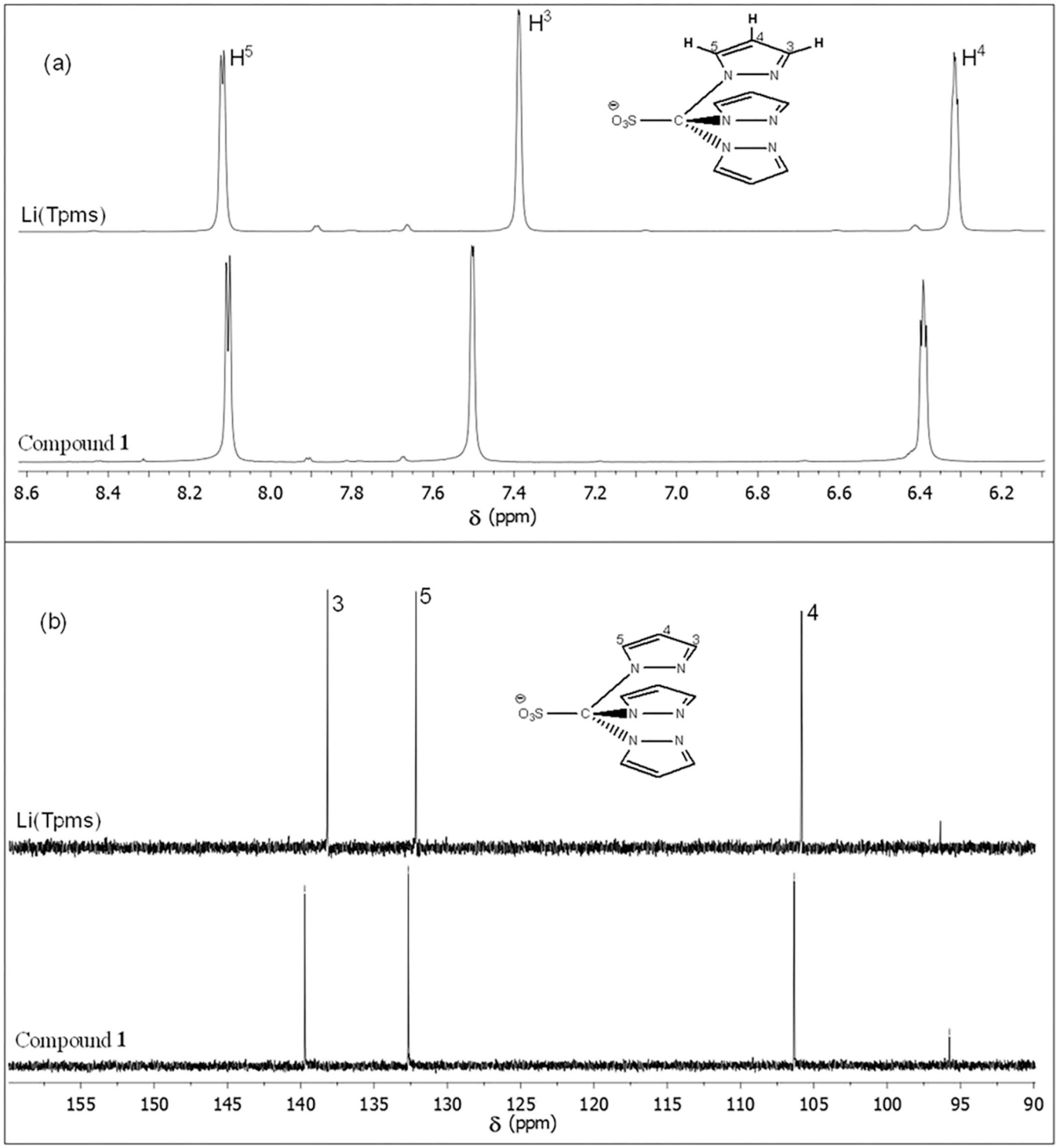

Fig. 1. ^{1}H NMR (a) and ^{13}C NMR and spectra of Li(Tpms) and compound **1** in DMSO-d_6.

Ag2-O3 of 2.864(7) Å, see Fig. 2 and legend] which, however, are shorter than the sum of the van der Waals radii of such atoms (1.72 Å for Ag and 1.52 Å for O). The tiniest *intra*chain Ag···Ag distance is of 4.619(5) Å, while the *inter*chain one reaches 8.112(8) Å). Further discussion of the structure is presented in the Supplementary Material file.

2.2. Antiproliferative assays

To evaluate the in vitro antiproliferative potential of **1**, the MTS assay (3-(4,5-dimethylthiazol-2-yl)-5-(3-carboxymethoxyphenyl)-2-(4-sulfophenyl)-2H-tetrazolium salt in the presence of phenazine methosulfate, PMS) was performed and the IC_{50} determined for two tumour lines, ovarian carcinoma cell line (A2780) and colorectal carcinoma cell line (HCT116) (Fig. 4 and Table 1). After 48 h, a high decrease in cell viability was achieved with the increase of complex concentrations (Fig. 4). This antiproliferative effect was much more pronounced for the ovarian carcinoma cell line (A2780) compared to colorectal carcinoma cell line (Fig. 4A and B). Indeed, a very low IC_{50} concentration was observed for that cell line (0.04 μM) compared to HCT116 cell line (4.73 μM) (Table 1).

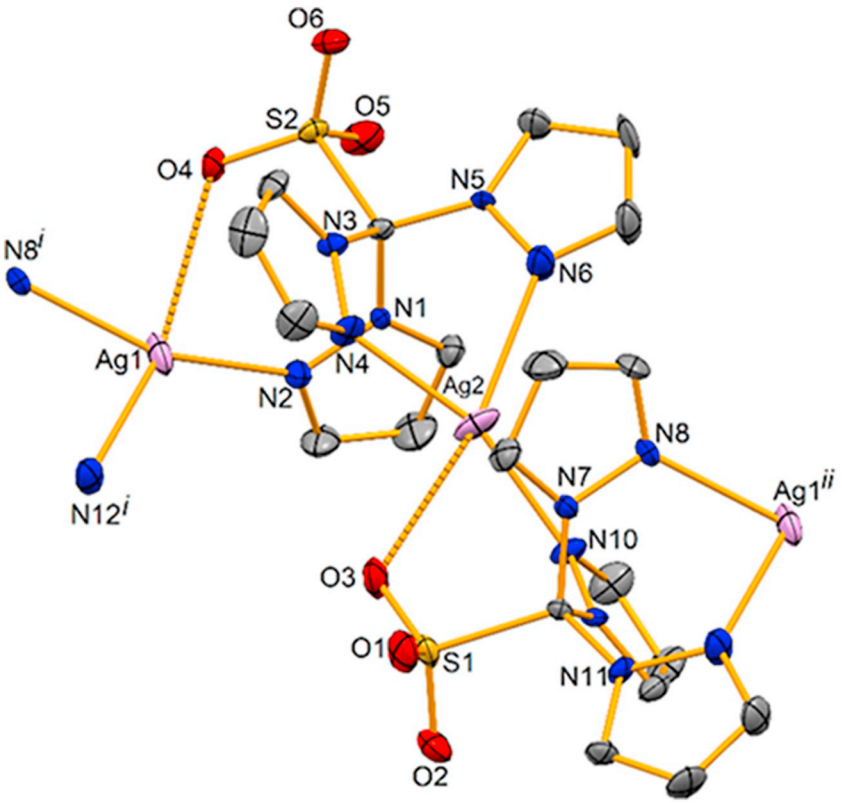

Fig. 2. ORTEP diagram of **1**, drawn at 30% probability level, with partial atom labelling scheme. Hydrogen atoms were omitted for clarity. Selected bond distances (Å) and angles (°): Ag1-N2 2.181(7), Ag1-N8^{i} 2.251(7), Ag1-N12^{i} 2.436(7), Ag1-O4 2.915(6), Ag2-N4 2.204(7), Ag2-N6 2.453(7), Ag2-N10 2.138(7), Ag2-O3 2.864(7), Ag1···Ag2 4.619(5), Ag2···Ag1^{ii} 4.703(5), N2-Ag1-N8^{i} 158.2(2), N2-Ag1-N12^{i} 123.9(2), N8^{i}-Ag1-N12^{i} 77.9(2), N4-Ag2-N6 79.0(2), N4-Ag2-N10 161.6(3), N6-Ag2-N10 119.3(2). Symmetry operations to generate the equivalent atoms: *i*) x,-1 + y,z; *ii*) x,1 + y,z.

The antiproliferative effect of **1** was also analysed in a normal human primary cell line - fibroblasts - as a way of evaluating the complex potential side effects in healthy cells (Fig. 5). A decrease of fibroblasts cell viability was also observed with the increase of complex concentration (similar to that observed with HCT116 line) (Figs. 4 and 5). As an additional way of evaluating the antiproliferative potential of **1**, the selectivity index based on the IC_{50} value of the tumour lines relative to the healthy fibroblasts was calculated [23]. As expected, the selectivity index is very high for the A2780 cell line, indicating that **1** is 129.5 times more selective for this cell line compared to normal human fibroblasts (Table 1). This result indicated that there is an interesting therapeutic window for using this compound as an antiproliferative agent in ovarian carcinoma derived cells.

The antiproliferative potential of silver(I) oxide (Ag_2O) and ligand (Li(Tpms)) were also analysed in A2780 cells individually and in combination. In all the concentrations tested the cell viability obtained was close to 100% proving that the antiproliferative effect observed in the presence of **1** is due to its action (Fig. 6).

The comparison between the cytotoxicity of compound **1** and other complexes in the literature containing Ag(I) or Tp/Tpm/Tpms ligands, reveals that **1** has a very high antiproliferative effect in A2780 and HCT116 cell lines [18,21,22]. Indeed, Silva and co-workers observed that treatment of HCT116 cell line with cobalt complexes bearing scorpionate ligands had no antiproliferative effect (IC_{50} at 48 h higher than 280 μM) [21]. In another study, Khan and co-workers prepared Ag (I) complexes with norharmane (9H-pyrido[3,4-*b*]indole) and observed IC_{50} values at 72 h in A2780 between 2.38 and 15.4 μM [24].

2.3. Variation in cell adhesion

A cell adhesion assay was performed to understand if there was any change in adhesion of A2780 cells after being in contact with **1**. One of the actions of silver is the ability to bind to proteins that exist in the membranes of both animal and bacterial cells [25]. This binding may alter the conformation of the membrane proteins affecting cell adhesion to the substrate. In this assay, A2780 adherent and non-adherent cells were counted and it was possible to distinguish between viable and non-viable cells. A2780 cells were counted after incubation in the presence of the IC_{50} of **1** or 0.1% DMSO (*v*/v) for 3, 24 and 48 h, and the results are shown in the Table 2.

As expected, there is a decrease of the percentage of viable adherent cells over time in the presence of **1** (Table 2). By contrast, there is an increase in the percentage of non-viable adherent A2780 cells. The

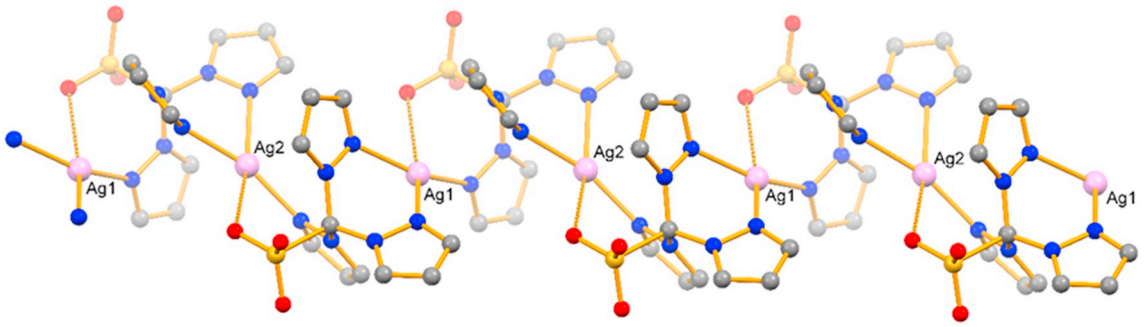

Fig. 3. Structural fragment of the helical chain of polymer 1, emphasised by the depth cue mode of representation.

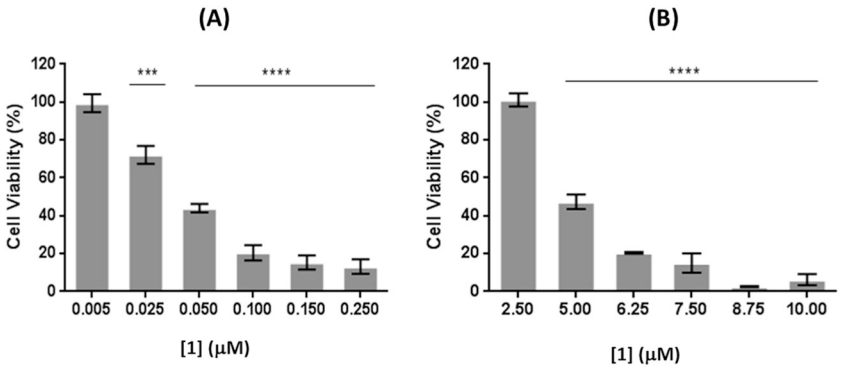

Fig. 4. Cell viability in A2780 **(A)** and HCT116 **(B)** tumour cell lines after 48 h exposure to compound **1**. Values of cell viability were normalized relative to the control vehicle (0.1% (v/v) DMSO). The values presented are the mean of three independent biological assays and the error bars correspond to the SEM. *P*-value was calculated using t-student comparing each concentration relative to the control (0.1% (*v*/v) DMSO) in each cell line. *** $p \leq 0.001$, **** $p \leq 0.0001$.

Table 1
Cytotoxicity of **1** represented by the relative IC_{50} in the A2780, HCT116 and fibroblasts cell lines. The antiproliferative activity was evaluated after 48 h of exposure. The selectivity index of **1** in the tumour cell lines were calculated. The data shown are expressed as the mean ± SEM of three independent biological assays.

Cell line	Relative IC_{50} (μM)	Selectivity index
A2780	0.04 ± 0.01	129.5
HCT116	4.73 ± 0.16	1.09
Fibroblasts	5.18 ± 0.10	–

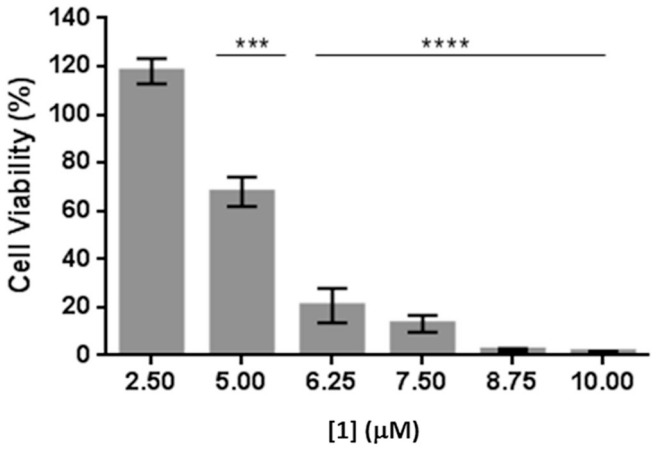

Fig. 5. Cell viability in normal human primary fibroblasts after 48 h of exposure to the compound **1**. Values of cell viability were normalized relative to the control vehicle (0.1% (v/v) DMSO). The values presented are the mean of three independent biological assays and the error bars correspond to the SEM. P-value was calculated using t-student comparing each concentration relative to the control (0.1% (v/v) DMSO) in each cell line. *** $p \leq 0.001$, **** $p \leq 0.0001$.

number of viable non-adherent cells remains near 10% independently of the incubation time (Table 2). This result demonstrates that the effect on adhesion is almost immediate and might be related to the release of silver ions from the compound [25,26]. This non incremental effect might probably be due to the fact that the silver ions originate Ag_2O and this oxide precipitates leaving the metal cations unavailable to interact with the proteins. Non-viable non-adherent cells exist at very low percentages except at 48 h where they reach 6%. In general, it is found that **1** lead to an increase in the number of non-adherent cells which, over time, are no longer viable (Table 2).

2.4. Cell death mechanism evaluation

As a preliminary analysis of the ability of **1** to induce apoptosis or necrosis, Hoescht 33258 and propidium iodide (PI) cellular staining

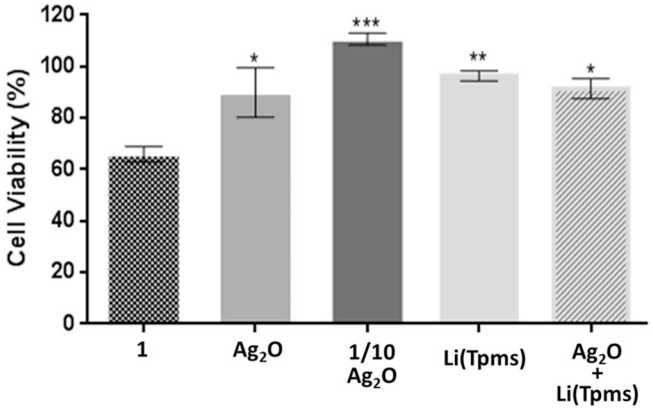

Fig. 6. Cell viability in A2780 cell line after 48 h exposure to **1**, Ag_2O, Tpms ligand and a combination of Ag_2O + Tpms. Values of cell viability were normalized relative to the control vehicle (0.1% (v/v) DMSO). The data are represented as mean ± SEM of three biological tests and statistical significance was evaluated in relation to the reference group (IC_{50} **1**) by the one-way ANOVA method (* $p \leq 0.05$, ** $p \leq 0.01$, *** $p \leq 0.001$).

was performed respectively, and results analysed by fluorescence microscopy. Cells in apoptosis or necrosis were counted after the incubation in the presence of the IC_{50} of **1** or 0.1% DMSO (*v*/v) (negative control) for 48 h. Fig. 7 shows representative images of each treatment. In the negative control, cells labelled with Hoescht show a homogeneous blue fluorescence distribution of chromatin throughout the nuclei (Fig. 7). Cells with this type of fluorescence distribution were considered viable [27]. Cells incubated with **1** show a non-homogeneous distribution of fluorescence with high fluorescence staining due to chromatin condensation and fragmentation – apoptotic cells (marked with an arrow) (Fig. 7) [27]. Indeed, in the presence of **1** about 40% of cells were apoptotic whereas in the negative control the value was close to 20%, meaning that there were twice as many cells with morphological alterations typical of cells in apoptosis when exposed to **1** (Fig. 8).

Regarding the labelling with the PI, no staining was observed in cells incubated with **1** (Fig. 7). This might indicate that **1** does not induce necrosis in A2780 after a 48 h exposition period.

In order to confirm the previous results, flow cytometry with dual labelling with annexin *V*-FITC and PI was used. This assay allows the quantification with high specificity and sensitivity of cells in apoptosis/necrosis. In this assay, annexin-V is conjugated to the Fluorescein isothiocyanate (FITC) fluorophore in order to detect attachment of annexin-V to phosphatidylserine (this phospholipid is found in the inner layer of the phospholipid bilayer being externalized in the early stages of apoptosis). As in early stages of apoptosis the plasma membrane has not yet lost its integrity the use of PI will allow distinguishing between cells in initial apoptosis and cells in late apoptosis, because it will not mark the first, but will mark the last ones where it can enter and bind to

Table 2
Variation of A2780 cell adhesion after 3, 24 or 48 h of exposure to the IC_{50} of **1**. Data are represented in percentages and expressed as the mean ± SEM of two independent biological assays.

	3 h		24 h		48 h	
	0.1% (*v*/v) DMSO	1 (IC_{50}; μM)	0.1% (v/v) DMSO	1 (IC_{50}; μM)	0.1% (v/v) DMSO	1 (IC_{50}; μM)
Viable Adherent Cells	91.8 ± 5.2	77.5 ± 7.1	88.6 ± 3.9	57.3 ± 11.2	85.8 ± 1.3	51.7 ± 5.0
Non-Viable Adherent Cells	7.6 ± 4.7	9.1 ± 2.6	10.5 ± 3.6	28.6 ± 6.1	12.9 ± 0.6	30.5 ± 2.1
Viable Non-Adherent Cells	0.6 ± 0.5	11.5 ± 2.8	0.9 ± 0.3	13.2 ± 4.6	1.3 ± 0.7	11.7 ± 5.3
Non-Viable Non-Adherent Cells	0	1.9 ± 1.7	0	0.9 ± 0.5	0	6.1 ± 1.7

DNA [28–30].

Cells were incubated with the IC_{50} of the compound for 48 h. As a negative control 0.1% DMSO (*v*/v) was used as a negative control and doxorubicin (0.4 μM; IC_{50}) was used as a positive control (due to its antitumor effect and induction of apoptosis) [31]. The negative control shows a 76% of viable cells, whereas in cells incubated with **1** there was a reduction in the number of viable cells to 49% with 47% of cells in early apoptosis and 4% of cells in late apoptosis. In the presence of doxorubicin, 60% of the cells were in early apoptosis and 13% cells in late apoptosis. Under all conditions the percentage of cells in necrosis was almost zero (Fig. 9). This is an interesting result since compounds that induce necrosis will lead to an increase in the level of inflammation in the tumour microenvironment while compounds inducing apoptosis lead to a programmed cell death with minimal damage and inflammation [32].

The changes in the mitochondrial membrane potential (ΔΨm) are a crucial parameter in the induction of apoptosis, mainly via the intrinsic pathway [33]. As a way of evaluating the change in ΔΨm, the lipophilic cationic probe tetraethylbenzimidazolylcarbocyanine iodide (JC-1) was used. In healthy cells with a high ΔΨm the JC-1 aggregates within the mitochondria emitting an intense red fluorescence signal. On the other hand, in cells with a low ΔΨm the JC-1 maintains its monomeric form in the cytoplasm presenting green fluorescence [34]. Fig. S6 shows representative images of the results obtained after 48 h of incubation in the presence of the IC_{50} of **1**, 0.1% DMSO (*v*/v) and untreated cells. In all cases, an intense red fluorescence signal was observed indicating that the cells have a high ΔΨm. Nevertheless, in the presence of **1** a slight increase in green fluorescence is observed in some cells, which may indicate a slightly change in the ΔΨm. This result may indicate that the ΔΨm change might not occur at an early stage of apoptosis but at a later stage. This might indicate that apoptosis is triggered via the extrinsic pathway [35].

Usually, the disruption of the mitochondrial membrane potential is associated with an increase of the ROS production. In our case, since there was almost no change in the ΔΨm in A2780 cell line, no generation of ROS is expected. For assessing that, a fluorescence assay was performed using 2,7-dichlorodihydrofluorescein diacetate (H2DCF-DA). H2DCF-DA is cleaved by the intracellular esterase into a non-fluorescent form (DCFH) which in the presence of ROS is oxidized to dichlorofluorescein (DCF) (fluorescence) which, in turn, is directly proportional to amount of ROS in cells [36]. H_2O_2 was used as a positive control. As expected, Fig. S7 shows that **1** did not induce the generation of ROS.

The intrinsic pathway of apoptosis is regulated by proteins of the B-cell lymphoma 2 (BCL-2) family, consisting of pro-apoptotic (e.g. BCL-2 associated protein, BAX) and anti-apoptotic (e.g. BCL-2) regulators [27]. An increase in the expression of BAX protein is associated with the induction of apoptosis by the intrinsic pathway, while increased expression of BCL-2 protein is associated with cell survival mechanism [37].

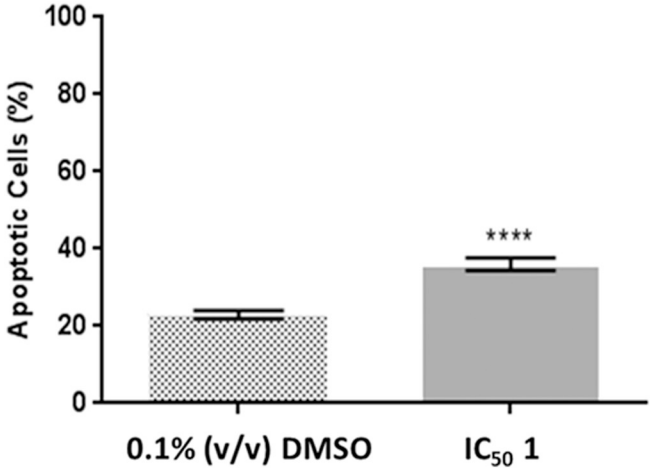

Fig. 8. Percentage of cells with typical morphological changes of apoptotic cells in the A2780 cell line after exposure to the IC_{50} of **1** for 48 h. Results are represented as the mean ± SEM of two independent biological assays and the statistical significance was evaluated in relation to the reference group (control) by the t-student method (**** $p \leq 0.0001$).

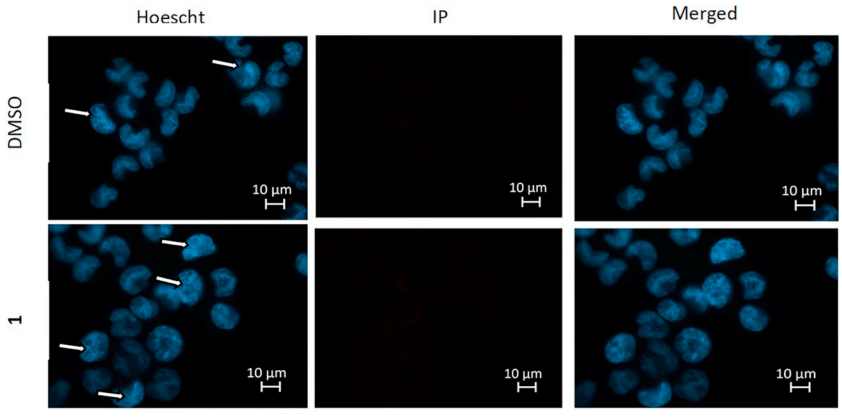

Fig. 7. A2780 tumour cell line labelled with Hoechst 33258 and PI for a visualization of apoptotic and necrotic cells, respectively. The cells were grown in the presence of 0.1% (v/v) DMSO (control) or the IC_{50} of **1** for 48 h. The arrows highlight those cells that present condensation and fragmentation of chromatin. The results were from two previous trials when at least 5 images were analysed for each condition under study.

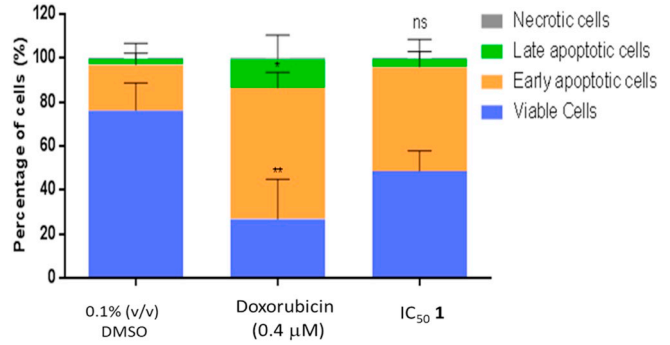

Fig. 9. Quantification of A2780 cells in apoptosis by flow cytometry with dual labelling with Annexin-FITC and PI. Cells were exposed to the IC_{50} of **1**, 0.1% (v/v) DMSO (control) or 0.4 µM of doxorubicin for 48 h. Data are represented as the mean ± SEM of two independent biological assays. Statistical significance was evaluated in relation to the reference group (control) by the two-way ANOVA method (* $p \leq 0.05$, ** $p \leq 0.01$, ns - statistically non-significant).

In Fig. 10 (A), the relative expression of BAX and BCL-2 proteins was measured after 48 h of incubation in the presence of the IC_{50} of **1** in A2780 cells. Although BAX protein expression is slightly higher than BCL-2 protein, this difference is not significant. The BAX/BCL-2 ratio [27,38] is close to one in control cells and in cells treated with **1** (Fig. 10 (B)) (e.g. BAX protein levels are identical to BCL-2 protein levels), which is consistent with the non-activation of the intrinsic pathway of apoptosis as observed above (Figs. 9, Fig. S6 and S7).

The results obtained so far indicate that apoptosis is triggered by **1** but possibly does not involve the intrinsic pathway.

Autophagy has emerged as an alternative process of cell death induced by several metal complexes [39]. Thus, to analyse the possible increase of autophagy due to **1**, the Cyto-ID probe, that stains with great precision autophagic compartments, was used. A2780 cells were incubated for 48 h with the IC_{50} of **1** or 0.1% DMSO (*v*/v) (negative control) or with 0.5 mM of rapamycin (positive control). Rapamycin serves as a positive control because it induces an increase in autophagy through inhibition of mammalian target of rapamycin (mTOR) [40]. As observed in Fig. 11, the autophagic compartments are all marked in green in the presence of **1** and rapamycin. This indicates that the induction of autophagy by **1** is comparable to the increase of autophagy caused by rapamycin (Fig. 11).

Co-activation of apoptosis and autophagy has been shown to occur with several metal compounds, except for some platinum compounds [41,42].

2.5. Cell cycle evaluation

The cytotoxicity of metal complex is often associated with DNA damage that can affect the cell cycle progression, leading to an accumulation of cells in the G1, S or G2/M phase [43]. The cytostatic potential of **1** in A2780 cells was analysed in G1/S phase synchronized cells (with a double thymidine block). Then, cells were incubated for 9, 12 and 24 h with the IC_{50} of **1** or 0.1% (*v*/v) DMSO in medium without thymidine to allow the cell cycle progression. The results were quantified by flow cytometry using PI (quantification of the DNA labelled per cell). Cells incubated in the presence of **1** follow the same pattern of the negative control, with no evidence of a delay in cell cycle progression (Table S2 and Fig. S8). This result indicates that **1** does not interfere with cell cycle progression either by interacting with proteins that control it or by leading to DNA damage that would lead to delay/blockage its progression.

2.6. Internalization of 1 in A2780 cells

Considering the previous results, we questioned if **1** was internalizing A2780 cells or if its action was mainly at the level of plasma membrane as indicated by the previous adhesion results (Table 2). Inductively coupled plasma – atomic emission spectrometry (ICP-AES) technique is a highly sensitive mass spectroscopy, that allows to determine extremely low concentrations of metals and several non-metals [44]. Considering this, cells were incubated for 3 h with 20 µM of **1** or 0.1% (v/v) DMSO in complete medium and the amount of silver quantified by ICP-AES in the supernatants and in cells lysates. In supernatants and cell lysates of control cells (0.1% (v/v) DMSO) no silver was detected as expected. Interestingly, concerning the cells incubated with **1**, 99% of the silver added to the cell medium was detected in the supernatants (only 1% was internalized). The results indicate that **1** does not substantially internalize tumour cells and its cytotoxicity might be related with damages occurring at the level of plasma membrane which agrees with the loss of viable adherent A2780 cells (Table 2) and the trigger of apoptosis via the extrinsic pathway.

2.7. Proteomic analysis of A2780 cells exposed to 1

In order to further characterize the cellular pathways affected by the presence of the IC_{50} of **1**, a comparative proteomic analysis of cells exposed for 48 h to the presence or absence of the complex was performed (Table 3 and Fig. 12). This technique, while intricate, provides a general idea of the cellular response of cells to different stress agents and allows confirming the results observed so far. The protein spots obtained in 2D gels were analysed in the Melanie 7.0 program to determine the variation of expression levels of the identified proteins and compared with a reference gel (Fig. S9) [45]. Proteins showing the most different expression levels between the presence and absence of **1** were excised, digested and characterized by matrix-assisted laser desorption/ionization coupled to time of flight (MALDI-TOF). Overall, 753 proteins were identified on the A2780 cell gels exposed to 0.1% (*v*/v) DMSO (control) and the **1** IC_{50}. Of these proteins, 51% had no changes in the expression levels and 49% showed variations, where 22% were sub-expressed and 27% were over-expressed (Fig. 12). The proteins identified and which exhibited differences in protein expression are shown in Table 3 and Fig. 12. Through bioinformatic analysis and databases, the identified proteins were classified based on their function. Classification of proteins in relation to their function was made using STRING 10.5 (Search Tool for the Retrieval of Interacting Genes/Proteins) and

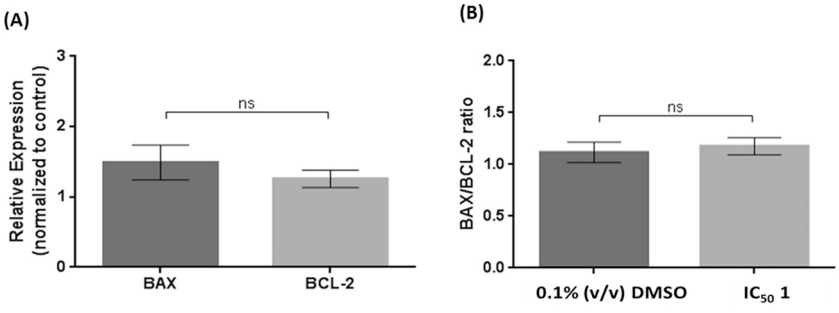

Fig. 10. (A) Levels of expression of BAX and BCL-2 on A2780 cells after 48 h incubation with the IC_{50} of **1**. **(B)** BAX/BCL-2 ratio in A2780 cells after incubation for 48 h with 0.1% (v/v) DMSO (control) and the IC_{50} of **1**. Relativized data compared to the control after normalization in relation to western blot of β-actin. Data are represented as the mean ± SEM of two independent assays and statistical significance was assessed by the t-student method (ns - statistically non-significant).

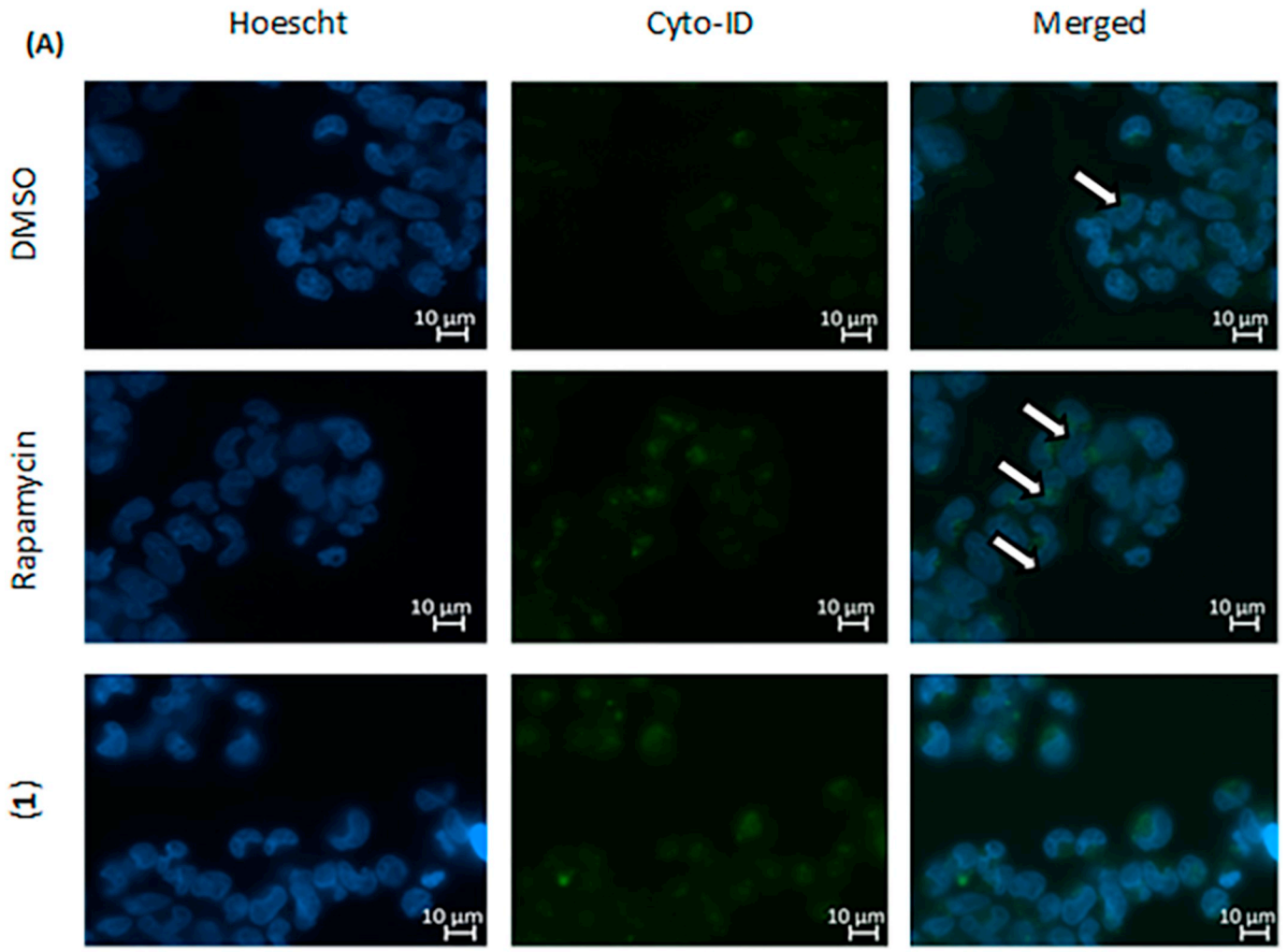

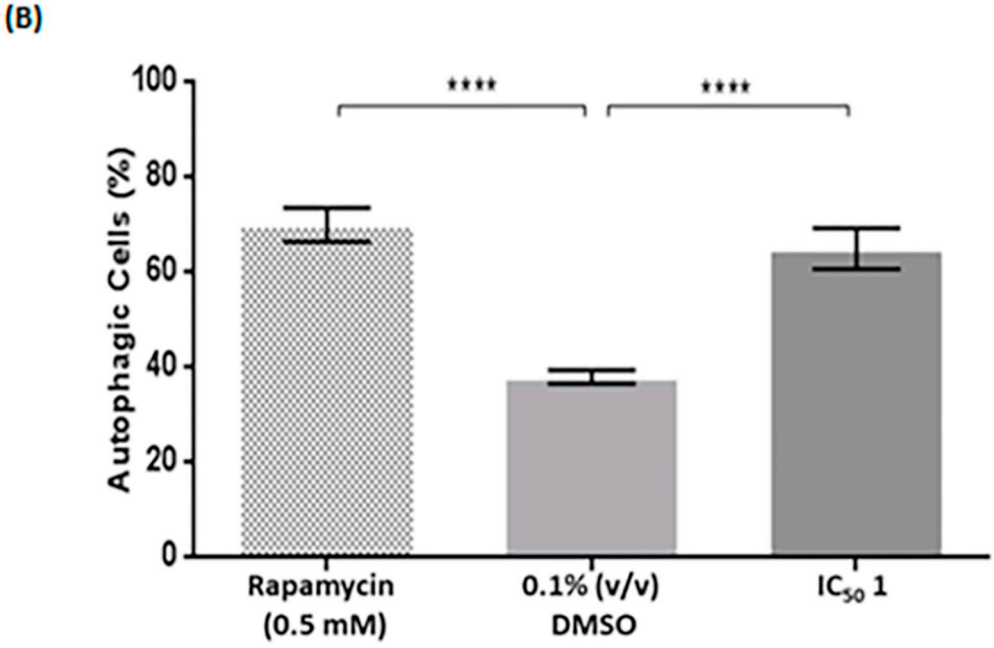

(caption on next page)

Fig. 11. (A) A2780 cells labelled with Cyto-ID probe for analysis of autophagic compartments. Cells were incubated with the IC_{50} of **1** or 0.1% (v/v) DMSO (control) for 48 h, or with 0.5 mM rapamycin (positive control) for 24 h. Cells with increased autophagosomes/autophagolysossomes are marked with an arrow. These results were obtained from two independent assays and at least 5 images were analysed for each condition under study. **(B)** Percentage of cells with autophagic compartments in A2780 cells. The results are represented as the mean ± SEM of two independent assays and the statistical significance was evaluated in relation to the control group (0.1% (v/v) DMSO) by the one-way ANOVA method (**** $p \leq 0.0001$).

UniProt (Universal Protein Resource).

The proteins affected by the addition of the compound were identified by significant differences in their expression compared to the control cell proteins. Within that group, most are related to stress responses and chaperonin proteins. Chaperonins are essential molecular complexes in protein folding. This rather diverse group of proteins has the function of protecting the cell. Thus, synthesis of chaperonins can be induced by physiological and pathological factors, such as thermal shock, oxidative stress, inflammation or infection. These proteins are present in the cytosol, mitochondria, endoplasmic reticulum, nucleus and plasma membrane [46]. An example of these proteins is the complex TCP1 (T-complex protein 1), constituted by the TCPA and TCPG subunits (among others) [47]. These proteins are over-expressed after incubation with **1**, which suggests an increased metabolism and folding of proteins in A2780 cells as a response to the stress to which they are subject under the influence of **1**.

ATP synthase F1 subunit beta, mitochondrial (ATP5B) is a protein involved in the catalysis of ATP synthesis in mitochondria [48]. The results indicate that, after exposure of the A2780 cells to the complex, it causes an over-expression of the ATP5B protein within the cell. This is probably due to the fact that in response to **1** stimulus, the metabolism of the cells differentiates in order to fight the alteration to which it is subjected, in this case increasing. In this sense, the over-expression of ATP5B may be the response of the cell to stress in the sense of providing ATP for all metabolic activities. This result is consistent with increased expression of the TCPA and TCPG proteins (which hydrolyse ATP) and the results obtained in previous assays where there was no change in the mitochondrial membrane potential and thus the mitochondria of the cells did not see their metabolic activity much affected. The sub-expression of Glutamate dehydrogenase 1, mitochondrial (DHE3) (enzyme involved in regulating metabolic activity [49]) and Leucine Aminopeptidase 3 (LAP3/AMPL) (protein involved in protein turnover [50]) may mean that the cell tries to maintain the metabolic homeostasis.

On the other hand, in the group of stress response proteins are heat shock proteins (HSP), including HSP90 and HSP70. The cells that incubated with **1** showed a sub-expression of the HSP70 and HSP90 proteins. According to the literature, the sub-expression of HSP70 is, in certain cases, enough to kill tumour cells but generally this under-expression aids the action of complexes that induce apoptosis [51]. HSP90 is involved in the regulation of post-translational and functional stabilization of several proteins known to be of vital importance in the tumour process. Due to this fact, there is currently intense research into therapies that may inhibit this protein [52]. The fact that **1** induces a sub-expression of HSP90 promotes a decrease in expression of essential proteins to the tumour cell, and consequently an increase in the stress of the A2780 cells. Regarding HSP70, its folding is aided by the co-chaperonin protein small glutamine-rich tetratricopeptide repeat-containing protein alpha (SGTA) [53], so the degree of expression of this will consequently affect the expression of HSP70. Thus, the results obtained, which point to its under-expression, will therefore be congruent with the diminutive expression of HSP70.

Another stress-response protein whose expression is altered is Annexin A2 (ANXA2). This protein is responsible for the regulation of the redox state of the cell, due to a cysteine residue that has in its constitution, easily oxidized by H_2O_2 [54]. Over-expression of this protein could mean that **1** induces oxidative stress in cells, although none of the assays performed corroborate this hypothesis. Thus, the increased expression observed may be related to an adaptive resistance response to the compound by the cell, since the ANXA2 protein is a drug resistance marker [55]. On the other hand, this increase may be associated with the over-expression of the ribosomal protein SA (RSSA), a ribosomal protein that is also involved in resistance to multiple drugs [56].

Calumenin (CALU) is a Ca^{2+} binding protein belonging to the (reticulocalbin and calumenin) CREC family. This protein is normally found in the endoplasmic reticulum; however, it can be transported into the cytoplasm after cell cycle arrest or in late apoptosis, being reduced

Table 3
Proteins identified on gels resulting from 2-D electrophoresis with expression variation relative to control (cells exposed for 48 h in the presence of **1** compared to the absence of **1**- see Fig. 12). Values smaller than 0.7 (red) were considered under-expression and values > 1.5 (green) were considered over-expression. Results are the mean of at least three independent 2-D gels for each condition.

Protein (Abbreviation)	Variation of expression	Molecular function
Cytosol aminopeptidase 3 (AMPL)	0.6	Turnover component
Annexin A2 (ANXA2)	1.9	Stress response
ATP synthase subunit beta (ATP5B)	3.9	Metabolism
Calumenin (CALU)	1.7	Metabolic processes of cellular proteins
Glutamate dehydrogenase 1 (DHE3)	0.6	Turnover component
Ezrin (EZRI)	0.6	Mobility of the cytoskeleton
Rho GDP-dissociation inhibitor 1 (GDIR1)	0.6	Control of homeostasis of Rho proteins
Heat shock cognate 71 kDa protein (HSP7C)	0.5	Stress and chaperone response
Heat shock protein HSP 90-beta (HSP90B)	0.4	Stress and chaperone response
Eukaryotic initiation factor 4A-I (IF4A1)	0.6	Sign translation
Pyrroline-5-carboxylate reductase 1 (P5CR1)	0.7	Stress response
Proliferation-associated protein 2G4 (PA2G4)	0.5	Regulation of growth
Proliferating cell nuclear antigen (PCNA)	0.4	Regulation of growth
Phosphoglycerate mutase 1 (PGAM1)	1.7	Glycolysis
Prohibitin (PHB)	3.6	Regulator of mitochondrial activity
Histone-binding protein RBBP7 (RBBP7)	3.3	Chromatin remodelling factor
40S ribosomal protein SA (RSSA)	1.9	Ribosome binding
Small glutamine-rich tetratricopeptide repeat-containing protein alpha (SGTA)	0.4	Stress and chaperone response
Stress-induced-phosphoprotein 1 (STIP1)	1.8	Connection to chaperone
T-complex protein 1 subunit alpha (TCPA)	2.8	Stress and chaperone response
T-complex protein 1 subunit gamma (TCPG)	3.6	Stress and chaperone response
T-complex protein 1 subunit theta (TCPQ)	0.2	Stress and chaperone response

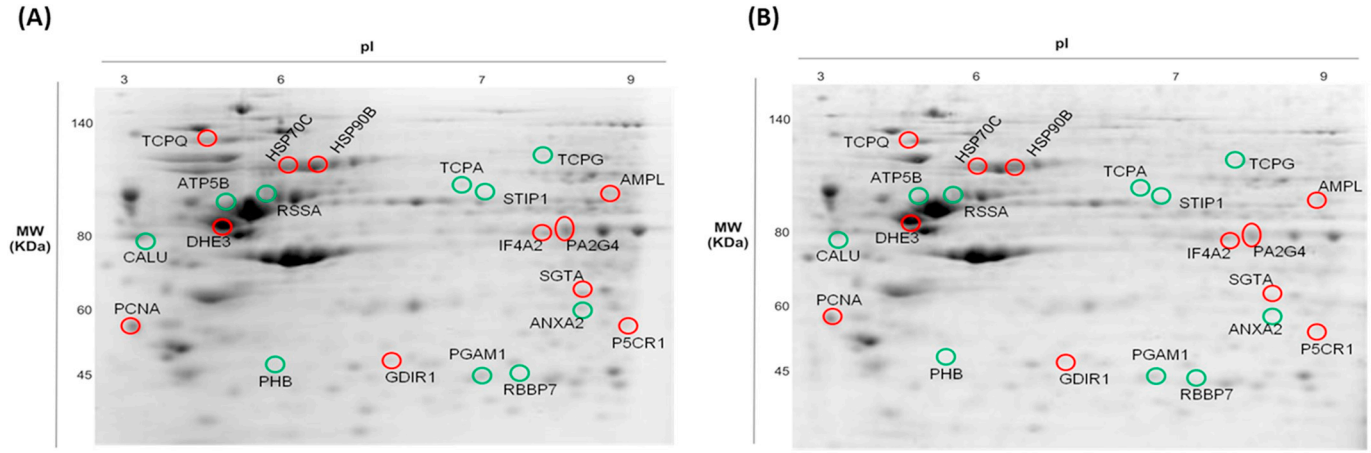

Fig. 12. 2-D Gels of protein extracts from A2780 tumour cells. Cells were incubated with **(A)** 0.1% (v/v) DMSO or **(B)** IC_{50} of **1** for 48 h. The gels were analysed in the Melanie 7.0 program. The spots identified represent proteins with their name acronym. The over-expressed proteins are represented by the green circles and the proteins sub-expressed by the circles in red. (For interpretation of the references to colour in this figure legend, the reader is referred to the web version of this article.)

in the cytoplasm during the early phase of apoptosis [57]. After exposure to **1**, an over-expression of this protein was observed in A2780 cells, indicating that the cells are undergoing apoptosis. This result, together with those of the double labelling with Annexin *V*-FITC and PI, seems to indicate that the cells are progressing between early and late apoptosis. Increased expression of prohibitin (PHB) protein also correlates with the induction of apoptosis in the presence of **1** [58]. Although the results indicate that the compound induces apoptosis via the extrinsic pathway the over-expression of the PHB protein may indicate some induction of apoptosis via the Bid protein.

Rhodopsin GDP-dissociation inhibitor 1 (GDIR1) plays an important role in the control of various cellular functions through interaction with the GTPase family in which rat sarcoma (Ras)-related C3 botulinum toxin substrate 1 (Rac1) is inserted. GDIR1 forms a complex with Rac1 preventing it from being cleaved by caspase 3 while keeping Rac1 in its active state. Thus, this protein is over-expressed in some types of tumour cells where it will promote cell resistance to apoptosis induced by chemotherapeutic agents [59]. In this case, the subexpression of GDIR1 indicates that the cells are susceptible to apoptosis induced by **1**, since the lack of GDIR1 leaves Rac1 exposed to cleavage by caspase 3, being this an essential event for the induction of apoptosis by a chemotherapeutic agent [59].

Finally, the proliferation-associated protein 2G4 (PA2G4) protein is involved in the Erb-B2 receptor tyrosine kinase 3 (ERBB3), also known as human epidermal growth factor receptor 3 (HER3)-regulated signal translation pathway and in promoting cell growth. It is composed of two isoforms: isoform 1 inhibits apoptosis and isoform 2 promotes cell proliferation [60]. As apoptosis occurs after incubation with the complex, the identified isoform should be 1 since there was a decrease in the expression of the protein which becomes insufficient to block apoptosis.

3. Experimental section

3.1. General Procedures and instrumentation

The synthetic procedure was performed in air, unless stated otherwise. Reagents and solvents were obtained from commercial sources and used without further purification. Li(Tpms) was synthesized using a reported method [13]. Carbon, hydrogen, nitrogen and sulphur elemental analyses were carried out by the Microanalytical services of the Instituto Superior Técnico. Infrared spectrum (4000–400 cm^{-1}) was obtained in a Cary 630 FTIR spectrometer; wavenumbers are in cm^{-1} (abbreviations: s, strong; m, medium; w, weak). Electrospray mass spectra (ESI-MS) were obtained with a *V*arian 500 MS LC Ion Trap Mass Spectrometer equipped with an electrospray ion source. For electrospray ionization, the drying gas and flow rate were optimized according to the particular sample with 35 p.s.i. nebulizer pressure. Both the negative and the positive modes were used (capillary voltage = 80–105 V). ^{1}H and ^{13}C NMR spectra were obtained using a Bruker Advance III 300 MHz UltraShield Magnet spectrometer, at ambient temperature; chemical shifts δ are quoted in ppm, and coupling constants given in Hz. Multiplicities are abbreviated as follows: doublet (d) and doublet of doublets (dd). ^{1}H and ^{13}C NMR spectra were internally referenced to the residual protio-solvent resonance and are reported relative to tetramethylsilane ($\delta = 0$). Assignments of some ^{1}H and ^{13}C signals rely on COSY and HSQC experiments.

3.2. Synthesis of $[Ag(Tpms)]_n$ (1)

A 50 mL Schlenk round bottom flask was charged with a solution of Li(Tpms) (100 mg, 0.33 mmol) in dry MeOH (10 mL). Under argon atmosphere, at room temperature and with continuous stirring, a solution of $AgNO_3$ (56 mg, 0.33 mmol) in 5 mL of dry MeOH was added; the solution immediately turned milky-white. While stirring for 3 h, a brick red precipitate was formed which was filtered off, washed with MeOH and dried in vacuum. By dissolving the product in MeCN and upon slow evaporation, compound **1** was afforded as colourless crystals suitable for SCXRD analysis.

Yield = 61%, based on silver (80 mg). Elemental analysis calcd (%) for $C_{10}H_9AgN_6O_3S{\cdot}0.4MeOH$ (413.70 g/mol): C 30.17, H 2.58, N 20.30, S 7.75; found: C 30.11, H 2.15, N 19.87, S 7.65. FTIR (KBr): ν (cm^{-1}) = 3479 w, 1651 m, 1519 m, 1419 m, 1382 m, 1319 s, 1243 s, 1196 m, 1096 m, 1064 m, 896 w, 861 s, 759 m, 367 s, 543 m. ^{1}H NMR (300 MHz, DMSO-d_6, δ): 8.10 (d, J = 2.4 Hz, 3H, 5-*H*-pz), 7.50 (d, J = 1.2 Hz, 3H, 3-*H*-pz), 6.39 (dd, J_1 = 2.4 Hz, J_2 = 1.2 Hz, 3H, 4-*H*-pz). $^{13}C\{^{1}H\}$ NMR (300 MHz, DMSO-d_6, δ): 139.72 (3-*C*-pz), 132.67 (5-*C*-pz), 106.75 (4-*C*-pz), 95.75 (CSO_3). ESI-MS^- in MeCN (*m/z* assignment, % intensity): 693 ($[Ag\{O_3SC(pz)_3\}_2]^-$, 100) 293 ($[O_3SC(pz)_3]^-$, 7). ESI-MS^+ in MeCN (*m/z* assignment, % intensity): 950 ($[Ag_3\{O_3SC(pz)_3\}_2(MeCN)]^+$, 51), 909 ($[Ag_3\{O_3SC(pz)_3\}_2]^+$, 63), 591 ($[Ag_2\{O_3SC(pz)_3\}(MeCN)_2]^+$, 100), 550 ($[Ag_2\{O_3SC(pz)_3\}(MeCN)]^+$, 62), 189 ($[Ag(MeCN)_2]^+$, 73), 148 ($[Ag(MeCN)]^+$, 14).

3.3. X-ray structure determination

A X-ray quality crystal of **1** was immersed in cryo-oil, mounted in a Nylon loop and measured at ambient temperature. Intensity data were

collected using a Bruker AXS-KAPPA APEX II PHOTON 100 diffractometer with graphite monochromated Mo-Kα (0.71069 Å) radiation. Data were collected using omega scans of 0.5° per frame and full sphere of data were obtained. Cell parameters were retrieved using Bruker SMART [61] software and refined using Bruker SAINT [61] on all the observed reflections. Absorption corrections were applied using the SADABS program [62]. The structure was solved by direct methods using SIR97 package [63] and refined with SHELXL-2014/7 [64]. Calculations were performed using the WinGX System-Version 2014.1 [65]. Least square refinements with anisotropic thermal motion parameters for all the non-hydrogen atoms and isotropic ones for the remaining atoms were employed. Crystallographic data and structure refinement details are provided in Table S1 and selected bond distances and angles in the legend of Fig. 2. CCDC 1914810 contains the supplementary crystallographic data for this paper. These data can be obtained free of charge from the Cambridge Crystallographic Data Centre.

3.3.1. Cell culture

Human ovarian carcinoma (A2780) cell line were grown in Roswell Park Memorial Institute medium (RPMI) (Invitrogen, New York, EUA) supplemented with 10% (*v*/v) foetal bovine serum and 1% (v/v) antibiotic/antimycotic solution (Invitrogen, New York, EUA) and maintained at 37 °C in a humidified atmosphere of 5% CO_2. Human colorectal carcinoma (HCT116) cell line and human primary fibroblasts were grown in Dulbecco's modified Eagle's medium (DMEM) (Invitrogen, New York, EUA) supplemented with 1% MEM non-essential amino acid (Sigma, St. Louis Missouri, EUA) and maintained at 37 °C in a humidified atmosphere of 5% CO_2. All cell lines were purchase from ATCC (www.atcc.org).

3.4. Viability assays

Cells were plated at 0.75×10^5 cells/well in 96-well plates. After 24 h the media was replaced with fresh media containing 0.005–0.25 μM of **1** for A2780 cell line and 2.5–10 μM of **1** for HCT116 cell line and fibroblasts or 0.1% (*v*/v) DMSO (vehicle, control). All the solutions were prepared from concentrated fresh stock solutions (in DMSO) of the complex. After 48 h of cell incubation in the presence or absence of **1**, metabolic viability was evaluated with CellTiter 96® AQueous Non-Radioactive Cell Proliferation Assay (Promega, Madison, WI, USA), using 3-(4,5-dimethylthiazol-2-yl)-5-(3-carboxymethoxyphenyl)-2-(4-sulfophenyl)-2H-tetrazolium, inner salt (MTS) as previously described in [27]. In brief, this is a homogeneous, colorimetric method for determining the number of viable cells. The CellTiter 96® AQueous Assay is composed of solutions of MTS and an electron coupling reagent (phenazine methosulfate, PMS). MTS is bioreduced by cells into a formazan product that is soluble in a tissue culture medium. The absorbance of the formazan product at 490 nm can be measured directly from 96-well assay plates without additional processing. The conversion of MTS into the aqueous soluble formazan product is accomplished by dehydrogenase enzymes found in metabolically active cells. The quantity of the formazan product was measured in a Tecan Infinite F200 Microplate Reader (Tecan, Männedorf, Switzerland) at 490 nm, as absorbance is directly proportional to the number of viable cells in culture.

3.4.1. Cell adhesion assays

As a way of evaluating the decrease in cell adhesion due to compound **1**, the Trypan blue exclusion method was used. Cells were plated at 7.5×10^4 cells/mL in 24-well plates with 24 h incubation. After that time the medium in which they were, was replaced by complete medium containing the IC_{50} of **1** or 0.1% (*v*/v) DMSO. Cells incubated for 3, 24 and 48 h. After each incubation period, the medium was removed and stored. To the cells in the well was added 300 μL of TrypLE™ Express (Gibco®, New York, USA), incubating for about 5 min. After detaching they were transferred to a centrifuge tube. To a 300 μL of the medium containing the cells and the cells transferred to the centrifuge tube were added 100 μL of Trypan blue. The cell concentration (cells/mL) of both viable and non-viable cells was obtained by multiplying the number of cells counted by the hemocytometer volume (10^4 mL^{-1}) and the dilution factor (400/300) divided by the number of quadrants where cells were counted.

3.4.2. Hoechst 33258 and PI labelling

A2780 cells were plated at 7.5×10^4 cells/mL in 24-well plates with 24 h incubation. After that time the medium in which they were, was replaced by complete medium containing the IC_{50} of **1** or containing 0.1% (*v*/v) DMSO. Cells incubated for 48 h. Following 48 h of treatment, cells were stained with Hoechst 33258 (excitation and fluorescence emission 352 and 461 nm, respectively) and IP (excitation and fluorescence emission 535 and 617 nm, respectively) in absence of light for 20 min, at 37 °C, as previously described in [18]. Fluorescent nuclei were analysed based on the chromatin condensation degree. Normal nuclei showed non-condensed chromatin uniformly distributed over the entire nucleus. Apoptotic nuclei showed condensate or fragmented chromatin. The samples were observed under the Olympus BX51 fluorescence microscope and photographed with an AXIO extension (Carl Zeiss, Oberkochen Germany), with 5 fields being taken with at least 100 cells counted per sample. The photographs were acquired and analysed in the ZEN Blue edition software (Carl Zeiss, Oberkochen Germany). The mean values presented were expressed as the percentage of apoptotic nuclei.

3.4.3. Annexin V-FITC/PI double-staining assay

A2780 cells were plated in 35 mm culture dishes at $7{,}5 \times 10^4$ cells/dish for 24 h. After this time the medium was replaced with complete medium containing the IC_{50} of the compound, 0.1% (*v*/v) DMSO, or doxorubicin (DOX) (0.4 μM) and the cells were incubated for 48 h in the same conditions referred to above. Afterwards, cells were collected and stained with PI and FITC labelled Annexin V according to the manufacturer's instructions (Annexin V-FITC Apoptosis Detection Kit; Invitrogen, USA) as previously described in [36]. The analysis and quantification of apoptosis were performed by flow cytometry on *Attune® Acoustic Focusing Flow Cytometer* (Life Technologies, Carlsbad, California) using an *Attune® Cytometric* software (Life Technologies), with the acquisition of at least 10 000 events per sample.

3.4.4. Alteration of mitochondrial membrane potential (ΔΨM)

To measure the mitochondrial membrane potential ($\Delta\Psi_M$) a lipophilic cationic dye − 5,5′,6,6′-tetrachloro-1,1′,3,3′-tetraethylbenzimidazolyl-carbocyanine iodide was used (JC-1; Abnova Corporation, Walnut, CA, USA). A2780 cells were plated at 7.5×10^4 cells/mL in 24-well plates with 24 h incubation. After this time the medium was replaced by the IC_{50} of the compound, 0.1% (*v*/v) DMSO in complete medium or medium for the corresponding untreated cells. Cells were incubated for 48 h under the above conditions. For evaluation of fluorescence intensity, cells were labelled with a JC-1 staining solution for 20 min at 37 °C in the dark. The samples were observed under the Olympus BX51 fluorescence microscope and photographed with an AXIO extension (Carl Zeiss, Oberkochen Germany), with 5 fields being taken with at least 100 cells counted per sample. The photographs were purchased by ZEN Blue edition software (Carl Zeiss, Oberkochen Germany) and analysed in ImageJ software (National Institutes of Health (NIH), Bethesda, MD, USA).

3.4.5. Production of intracellular reactive oxygen species (ROS)

A2780 cells were plated at 7.5×10^4 cells/mL in 24-well plates with 24 h incubation. After this time the medium was replaced by the IC_{50} of the compound, 0.1% (*v*/v) DMSO or 25 μM of H_2O_2 (positive control) in complete medium. After 48 h, cells were stained with ROS Detection Reagents (Life Technologies, Invitrogen™, USA) for 20 min at 37 °C,

protected from light. Data were obtained under the Olympus BX51 fluorescence microscope and photographed with an AXIO extension (Carl Zeiss, Oberkochen Germany), with 5 fields being taken with at least 100 cells counted per sample. The photographs were purchased by ZEN Blue edition software (Carl Zeiss, Oberkochen Germany) and analysed in ImageJ software (National Institutes of Health (NIH), Bethesda, MD, USA).

3.4.6. Apoptotic proteins expression by Western Blot

A2780 cells were seeded at 4×10^6 cells/mL in a 75 cm^2 cell culture flask and incubated for 24 h. After that time the medium in which they were, was replaced by complete medium containing the IC_{50} of **1** or containing 0.1% (*v*/v) DMSO. After 48 h of treatment, the whole protein extract was obtained as described in [66]. The membrane was incubated for 1 h with fresh 5% non-fat milk in 1 × Tris-buffer saline with Tween-20 (TBST) (50 mM Tris, 150 mM NaCl and 0,1% (v/v) Tween 20, pH ~7.5) to block non-specific protein bidding. Then, each nitrocellulose membrane was exposed to different primary antibody in 5% non-fat milk in TBST, namely anti-Bax (1:5000; Abcam, United Kingdom) and anti Bcl-2 (1:1000; Sigma, St. Louis, EUA) and was left to incubate for 1 h at RT, with constant agitation. Next, the membrane was washed three times with 1 × TBST buffer with agitation for 5 min at RT. The same procedure above was also employed to the membrane incubation with the secondary antibody (1:3000, Anti-mouse IgG, horseradish peroxidase (HPR)-linked Antibody or 1:2000, Anti-rabbit IgG, HPR-linked Antibody; Cell Signaling Technology, USA). All membranes were stripped with stripping buffer (0.1 M glycine, 20 mM magnesium acetate and 50 mM potassium chloride) and, then, re-incubated with anti-ß actin (1:5000; Sigma, St. Louis, EUA) as a control for further normalization of the results. To detect the protein bands, a WesternBright Excellent Chemiluminescent (ECL) subtract (Advansta, USA) was prepared and membranes incubated for 5 min. Next, the film was exposed to the membrane, on a dark room. The quantification of proteins was determinate by densitometry using *Image J* software.

3.4.7. Autophagic potential

For the detection of autophagy in the A2780 cell line the CYTO-ID® Autophagy Detection Kit (Enzo Life Sciences, UK) was used. The A2780 cells were cultured at a cell concentration of 7.5×10^4 cells/mL, for 24 h in order to adhere. After this period the medium was replaced by medium containing the IC_{50} of the compound, 0.1% (*v*/v) DMSO or 5 μL of a 50 mM solution of rapamycin (positive control). After 48 h of incubation, the medium was removed and cells were stained according to the instructions of the CYTO-ID® Autophagy Detection Kit (Enzo Life Sciences, UK). The samples were observed under the Olympus BX51 fluorescence microscope and photographed with an AXIO extension (Carl Zeiss, Oberkochen Germany), with 5 fields being taken with at least 100 cells counted per sample. The photographs were acquired and analysed in the ZEN Blue edition software (Carl Zeiss, Oberkochen Germany).

3.4.8. Cell cycle progression

For analysis, A2780 cells were grown in 6-well plates at a cell concentration of 1×10^5 cells/mL and incubated at 37 °C, 5% CO_2 and 99% humidity relative. Cells were synchronized by a double thymidine block (2 mM) (Sigma, St. Louis, USA) as described in [36]. Cells were released from the second block by substituting with fresh medium containing the IC_{50} of the **1**, or 0.1% (*v*/v) DMSO for 9, 12 and 24 h. For synchronization control purpose, cells from another disk were collected after thymidine block. After each time point, cells were collected and treated with 50 μg/mL RNase A for 30 min at 37 °C and, then with PI (2.5 μg/mL). The DNA content was analysed on Attune® Acoustic Focusing Flow Cytometer (Applied Biosystems) and the data were treated with *FCS Express 6 Flow Cytometry* software.

3.4.9. Silver detection

As a way of evaluating the entry of the compound into the cell, the inductive coupled plasma mass spectrometry (ICP-AES) technique was used through a contracted service. For the preparation of the samples the A2780 cells were cultured in 25 cm^2 culture flasks at a cell density of 5×10^5 cells/mL and incubated at 37 °C, 5% CO_2 and 99% relative humidity, for 24 h. After this period the medium was replaced with a solution of **1** at 20 μM or 0.1% (v/v) DMSO in complete medium and incubated for 3 h. Then the medium was removed and stored at −20 °C. To the cells in the culture flask was added 2 mL TrypLE™ Express (Gibco®, New York, USA), incubating for about 5 min at RT. After detachment, the cells were transferred to 15 ml Falcon tubes and centrifuged for 5 min at 700 x*g* and 20 °C. The supernatant is discarded, and the cell pellet is stored at −20 °C. One day before the samples are submitted for analysis, freshly prepared aqua regia is added.

3.4.10. Comparative proteomic analysis

A2780 cells were seeded at 4×10^6 cells/mL in a 75 cm^2 cell culture flask and incubated for 24 h. After that time the medium in which they were, was replaced by complete medium containing the IC_{50} of **1** or 0.1% (*v*/v) DMSO. After 48 h of treatment, the whole protein extract was obtained as described in [66]. For whole protein precipitation and purification 2-D Clean-Up Kit (GE Healthcare, United Kingdom) was used accordingly with manufacturer's protocol (Healthcare, 2009) with exception for wash additive and wash buffer step, where cell lysates were incubated overnight at −20 °C. After centrifugation, 120 μL of rehydration buffer (7 M urea (BDH Prolabo, VWR International), 2 M Thiourea (Merck, Frankfurt, Germany), 2% (*w*/*v*) 3-[(3-Cholamidopropyl) dimethyl ammonia]-1 propane sulfonate (GE Healthcare, United Kingdom), phosphatase inhibitors 1 ×, protease inhibitors 1 ×, bromophenol blue (Merck, Frankfurt, Germany), 0.1% (w/v) DTT and 1 mM PMSF) were added to protein extract, and allowed to react overnight at RT. Finally, the samples were centrifuged at 12,000 × *g* for 10 min, recovering the supernatants. For total protein quantification, Pierce Protein Assay kit (ThermoScientific) was used.

Isoelectric focusing (IEF), was performed using Immobiline DryStrip pH 3–10, 7 cm (GE Healthcare, United Kingdom) in an Ettan IPGphor3 IEF focusing unit (GE Healthcare, United Kingdom). Before sodium dodecyl sulphate – polyacrylamide gel electrophoresis (SDS-PAGE), immobilized pH gradient (IPG) strips were incubated into two equilibrium solutions to assure the protein's primary structural conformation. Initially, strips were loaded onto an equilibrium solution (70 mM Tris-HCl pH 8.8, 6 M Urea, 30% (v/v) glycerol and 2% (w/v) SDS (GE Healthcare, United Kingdom)) supplemented with 1% (w/v) DTT for 15 min at RT, followed by a second solution further supplemented with 2.5% (w/v) iodoacetamide (GE Healthcare, United Kingdom), incubated for another 15 min under constant stirring. SDS-PAGE was performed in 12.5% (v/v) polyacrylamide gel in a SDS-PAGE Mini-PROTEAN® 3 System (BioRad). The resulting gels were stained with Coomassie R350 (GE Healthcare). The gels were scanned using the PIXMA M250 scanner (Canon) and analysed in the Melanie 7.0 program (GeneBio, Geneva, Switzerland). The analysis was performed by automatic spot detection, identification of protein spots, spot matching between different gels and determination of intensity/expression of each spot. The variation in the expression levels of each protein was calculated from the ratio of the intensity of each of the spots of the samples by the intensity of each spot of the controls, as described in [45]. To confirm the correct translations from the reference map and to identify other differentially expressed proteins of interest, protein spots were manually excised from the gel and identified in the UniMS – Mass Spectrometry Unit, ITQB/IBET (Oeiras, Portugal) using Peptide Mass fingerprint.

3.5. Statistical analysis

All results were expressed as mean ± Standard error of the mean (SEM) of at least three independent biological assays with technical

triplicates each. The program GraphPad Prism 6 software was used in the analysis of results through One or Two-way ANOVA or Student's *t*-test in order to compare the control group with the treated groups for statistical significance. Results with a $p < 0.05$ were considered statistically significant.

4. Conclusions

The characterization of the antiproliferative potential of the silver(I) tris(pyrazolyl)methane sulfonate compound was performed on two human tumour cell lines, viz. A2780 and HCT116. An antiproliferative effect in both cell lines was disclosed. However, the antiproliferative activity of **1** in A2780 cell line is much higher (IC_{50} of 0.04 μM) compared to the HCT116 cell line. The antiproliferative effect of **1** in non-tumour cells - fibroblasts was similar to that observed for HCT116 cells, but an interesting therapeutic window compared to A2780 cells exists, and thus this cell line was selected for further biological assays. Considering the high antiproliferative activity of **1** we have shown that: 1) it interferes with the adherence of A2780 cells being this effect almost immediate and most likely related to the release of silver ions from the compound; 2) the main mechanism of cell death activated by the compound is apoptosis. To understand if this trigger of apoptosis occurred via the intrinsic or extrinsic pathway, mitochondrial membrane potential, the increase in the production of ROS and the changes in the expression of pro- and anti-apoptotic proteins, BAX and BCL-2 respectively, were analysed, demonstrating that most probably the mitochondria/intrinsic process was not involved (unless through Bid protein) and pointing out to an induction of apoptosis via the extrinsic pathway. This hypothesis was supported by the results obtained via ICP-AES technique in which silver was detected only in the A2780 supernatants. Results also indicated that another mechanism of cell death via autophagy was triggered. However, further studies are needed because the increase in autophagy is the response of the cell to stress and may end up having two opposite results: serve as a cellular mechanism for survival or induce cell death. The cytostatic potential of **1** was excluded as it did not appear to affect the progression of the cell cycle. Finally, the proteomic analysis allowed us to identify two types of A2780 cell response to compound **1**: the first response supports its antiproliferative activity, where cells activates mechanisms to trigger apoptosis and a second cellular response related to counter act the stress induced by **1** by increasing the metabolism via enhancing ATP production, protein synthesis and resistance to stress.

Acknowledgments

This work was financed by national funds from the Foundation for Science and Technology FCT/MCTES (UID/Multi/04378/2019 and UID/QUI/00100/2019), Portugal, and supported by the Applied Molecular Biosciences Unit- UCIBIO, and by the Centro de Química Estrutural (CQE at IST). AGM is thankful to the CATSUS doctoral program of FCT/MCTES for his PhD fellowship (SFRH/BD/106006/2014). The authors acknowledge the Portuguese NMR Network (IST-UL Centre) for access to the NMR facility and the IST Node of the Portuguese Network of Mass-spectrometry for the ESI-MS measurements. CRR also acknowledges FCT/MCTES through SFRH/BPD/124612/2016. LMDRSM acknowledges FCT/MCTES through PTDC/QEQ-ERQ/1648/2014.

Appendix A. Supplementary data

Supplementary data to this article can be found online at https://doi.org/10.1016/j.jinorgbio.2019.110789.

References

[1] R.A. Weinberg, The Biology of Cancer, 2nd ed., W. W. Norton & Company, 2013.
[2] L. Pecorino, Molecular biology of cancer: mechanisms, targets, and therapeutics, Oxford university press, 2012. https://www.google.com/books?hl=en&lr=&id=tI_vcU85QU4C&oi=fnd&pg=PP1&dq=Molecular+Biology+of+Cancer:+Mechanisms,+Targets,+and+Therapeutics&ots=VL1qTv7tzm&sig=xuFUYMoCEIJimNfjB9fbnGqtgDM (accessed May 6, 2019).
[3] World Health Organization, WHO, https://www.who.int/cancer/en/, (2019) (accessed May 6, 2019).
[4] P.G. Corrie, Cytotoxic chemotherapy: clinical aspects, Medicine (Baltimore) 39 (2011) 717–722, https://doi.org/10.1016/J.MPMED.2011.09.012.
[5] B. Rosenberg, E. Renshaw, L. Vancamp, J. Hartwick, J. Drobnik, Platinum-induced filamentous growth in Escherichia coli, J. Bacteriol. 93 (1967) 716–721 http://www.ncbi.nlm.nih.gov/pubmed/5335970 , Accessed date: 6 May 2019.
[6] J. Silva, A.S. Rodrigues, P.A. Videira, J. Lasri, A.J. Charmier, A.J.L. Pombeiro, A.R. Fernandes, Characterization of the antiproliferative potential and biological targets of a trans ketoimine platinum complex, Inorganica Chim. Acta. 423 (2014) 156–167, https://doi.org/10.1016/J.ICA.2014.07.067.
[7] U. Ndagi, N. Mhlongo, M.E. Soliman, Metal complexes in cancer therapy - an update from drug design perspective, Drug Des. Devel. Ther. 11 (2017) 599–616, https://doi.org/10.2147/DDDT.S119488.
[8] M. Frezza, S. Hindo, D. Chen, A. Davenport, S. Schmitt, D. Tomco, Q. Ping Dou, Novel metals and metal complexes as platforms for cancer therapy, Curr. Pharm. Des. 16 (2010) 1813–1825, https://doi.org/10.2174/138161210791209009.
[9] D.A. Medvetz, K.M. Hindi, M.J. Panzner, A.J. Ditto, Y.H. Yun, W.J. Youngs, Anticancer activity of Ag(I) N-heterocyclic carbene complexes derived from 4,5-dichloro-1H-imidazole, Met. Based. Drugs. 2008 (2008), https://doi.org/10.1155/2008/384010.
[10] S. Medici, M. Peana, G. Crisponi, V.M. Nurchi, J.I. Lachowicz, M. Remelli, M.A. Zoroddu, Silver coordination compounds: a new horizon in medicine, Coord. Chem. Rev. 327–328 (2016) 349–359, https://doi.org/10.1016/J.CCR.2016.05.015.
[11] U. Kalinowska-Lis, A. Felczak, L. Chęcińska, I. Szabłowska-Gadomska, E. Patyna, M. Małecki, K. Lisowska, J. Ochocki, U. Kalinowska-Lis, A. Felczak, L. Chęcińska, I. Szabłowska-Gadomska, E. Patyna, M. Małecki, K. Lisowska, J. Ochocki, Antibacterial activity and cytotoxicity of silver(I) complexes of pyridine and (Benz) imidazole derivatives. X-ray crystal structure of [Ag(2,6-di(CH2OH)py)2]NO3, Molecules 21 (2016) 87–101, https://doi.org/10.3390/molecules21020087.
[12] S. Trofimenko, Boron-pyrazole chemistry. I. Prrazaboles, J. Am. Chem. Soc. 89 (1967) 3165–3170, https://doi.org/10.1021/ja00989a016.
[13] W. Kläui, M. Berghahn, G. Rheinwald, H. Lang, Tris(pyrazolyl)methanesulfonates: a novel class of water-soluble ligands, Angew. Chemie Int. Ed. 39 (2000) 2464–2466, https://doi.org/10.1002/1521-3773(20000717)39:14<2464::AID-ANIE2464>3.0.CO;2-5.
[14] G. Paula, P. Smolenski, Ligands: synthesis, characterization and role in biotechnology, Biochem. Res. Trends, Nova Science Publishers, Incorporated, 2014.
[15] W. Kläui, D. Schramm, W. Peters, G. Rheinwald, H. Lang, Tris(pyrazolyl)methanesulfonate (Tpms) − a versatile alternative to Tris(pyrazolyl)borate in rhodium(I) chemistry, Eur. J. Inorg. Chem. 2001 (2001) 1415–1424, https://doi.org/10.1002/1099-0682(200106)2001:6<1415::AID-EJIC1415>3.0.CO;2-Z.
[16] L.M.D.R.S. Martins, A.J.L. Pombeiro, Water-soluble C-scorpionate complexes-catalytic and biological applications, Eur. J. Inorg. Chem. 2016 (2016) 2236–2252, https://doi.org/10.1002/ejic.201600053.
[17] E.T. Papish, M.T. Taylor, F.E. Jernigan, M.J. Rodig, R.R. Shawhan, G.P.A. Yap, F.A. Jové, Synthesis of zinc, copper, nickel, cobalt, and iron complexes using tris(pyrazolyl)methane sulfonate ligands:a structural model for N,N,O binding in metalloenzymes, Inorg. Chem. 45 (2006) 2242–2250, https://doi.org/10.1021/IC051579A.
[18] F. Silva, C. Fernandes, M.P.C. Campello, A. Paulo, Metal complexes of tridentate tripod ligands in medical imaging and therapy, Polyhedron, in press, doi:https://doi.org/10.1016/j.poly.2016.11.040.
[19] V. Gandin, F. Tisato, A. Dolmella, M. Pellei, C. Santini, M. Giorgetti, C. Marzano, M. Porchia, In vitro and in vivo anticancer activity of copper(I) complexes with homoscorpionate tridentate tris(pyrazolyl)borate and auxiliary monodentate phosphine ligands, J. Med. Chem. 57 (2014) 4745–4760, https://doi.org/10.1021/jm500279x.
[20] J. Niesel, A. Pinto, H.W.P. N'Dongo, K. Merz, I. Ott, R. Gust, U. Schatzschneider, Photoinduced CO release, cellular uptake and cytotoxicity of a tris(pyrazolyl)methane (tpm) manganese tricarbonyl complex, Chem. Commun. 15 (2008) 1798–1800, https://doi.org/10.1039/b719075a.
[21] T.F.S. Silva, L.M.D.R.S. Martins, M.F.C.G. da Silva, A.R. Fernandes, A. Silva, P.M. Borralho, S. Santos, C.M.P. Rodrigues, A.J.L. Pombeiro, Cobalt complexes bearing scorpionate ligands: synthesis, characterization, cytotoxicity and DNA cleavage, Dalton Trans. 41 (2012) 12888–12897, https://doi.org/10.1039/c2dt11577h.
[22] C. Pettinari, F. Marchetti, G. Lupidi, L. Quassinti, M. Bramucci, D. Petrelli, L.A. Vitali, M.F.C. Guedes da Silva, L.M.D.R.S. Martins, P. Smolenski, A.J.L. Pombeiro, Synthesis, antimicrobial and antiproliferative activity of novel silver(I) tris(pyrazolyl)methanesulfonate and 1,3,5-Triaza-7-phosphadamantane complexes, Inorg. Chem. 50 (2011) 11173–11183, https://doi.org/10.1021/ic201714c.
[23] K. Czerwińska, B. Machura, S. Kula, S. Krompiec, K. Erfurt, C. Roma-Rodrigues, A.R. Fernandes, L.S. Shul'pina, N.S. Ikonnikov, G.B. Shul'pin, Copper(ii) complexes of functionalized 2,2′:6′,2″-terpyridines and 2,6-di(thiazol-2-yl)pyridine: structure, spectroscopy, cytotoxicity and catalytic activity, Dalton Trans. 46 (2017) 9591–9604, https://doi.org/10.1039/C7DT01244F.
[24] R.A. Khan, K. Al-Farhan, A. de Almeida, A. Alsalme, A. Casini, M. Ghazzali, J. Reedijk, Light-stable bis(norharmane)silver(I) compounds: synthesis, characterization and antiproliferative effects in cancer cells, J. Inorg. Biochem. 140 (2014)

1–5, https://doi.org/10.1016/j.jinorgbio.2014.06.019.
[25] A.B.G. Lansdown, Silver I: its antibacterial properties and mechanism of action, J. Wound Care 11 (2002) 125–130, https://doi.org/10.12968/jowc.2002.11.4.26389.
[26] M.A. Iqbal, R.A. Haque, S.F. Nasri, A.A. Majid, M.B.K. Ahamed, E. Farsi, T. Fatima, Potential of silver against human colon cancer: (synthesis, characterization and crystal structures of xylyl (Ortho, meta, & Para) linked bis-benzimidazolium salts and Ag(I)-NHC complexes: in vitro anticancer studies), Chem. Cent. J. 7 (2013) 27, https://doi.org/10.1186/1752-153X-7-27.
[27] Z. Ma, B. Zhang, M.F.C. Guedes da Silva, J. Silva, A.S. Mendo, P.V. Baptista, A.R. Fernandes, A.J.L. Pombeiro, Synthesis, characterization, thermal properties and antiproliferative potential of copper(ii) 4′-phenyl-terpyridine compounds, Dalton Trans. 45 (2016) 5339–5355, https://doi.org/10.1039/C5DT02744F.
[28] E. Hollville, S.J. Martin, Measuring apoptosis by microscopy and flow cytometry, Curr. Protoc. Immunol, John Wiley & Sons, Inc., Hoboken, NJ, USA, 2016, pp. 14.38.1–14. 38.24, , https://doi.org/10.1002/0471142735.im1438s112.
[29] G. Brumatti, C. Sheridan, Expression and purification of recombinant annexin V for the detection of membrane alterations on apoptotic cells, Methods 44 (2008) 235–240, https://doi.org/10.1016/J.YMETH.2007.11.010.
[30] P. Brun, B. Zavan, V. Vindigni, A. Schiavinato, A. Pozzuoli, C. Iacobellis, G. Abatangelo, *In vitro* response of osteoarthritic chondrocytes and fibroblast-like synoviocytes to a 500-730 kDa hyaluronan amide derivative, J. Biomed. Mater. Res. Part B Appl. Biomater. 100B (2012) 2073–2081, https://doi.org/10.1002/jbm.b.32771.
[31] S. Fulda, K.-M. Debatin, Extrinsic versus intrinsic apoptosis pathways in anticancer chemotherapy, Oncogene 25 (2006) 4798–4811, https://doi.org/10.1038/sj.onc.1209608.
[32] S.W.G. Tait, G. Ichim, D.R. Green, Die another way–non-apoptotic mechanisms of cell death, J. Cell Sci. 127 (2014) 2135–2144, https://doi.org/10.1242/jcs.093575.
[33] R. Singh, A. Letai, K. Sarosiek, Regulation of apoptosis in health and disease: the balancing act of BCL-2 family proteins, Nat. Rev. Mol. Cell Biol. 20 (2019) 175–193, https://doi.org/10.1038/s41580-018-0089-8.
[34] A. Perelman, C. Wachtel, M. Cohen, S. Haupt, H. Shapiro, A. Tzur, JC-1: alternative excitation wavelengths facilitate mitochondrial membrane potential cytometry, Cell Death Dis. 3 (2012) 430–437, https://doi.org/10.1038/cddis.2012.171.
[35] J.D. Ly, D.R. Grubb, A. Lawen, The mitochondrial membrane potential (Δψm) in apoptosis; an update, APOPTOSIS 8 (2003) 115–128, https://doi.org/10.1023/A:1022945107762.
[36] A. Silva, D. Luís, S. Santos, J. Silva, A.S. Mendo, L. Coito, T.F.S. Silva, M.F.C.G. da Silva, L.M.D.R.S. Martins, A.J.L. Pombeiro, P.M. Borralho, C.M.P. Rodrigues, M.G. Cabral, P.A. Videira, C. Monteiro, A.R. Fernandes, Biological characterization of the antiproliferative potential of co(II) and Sn(IV) coordination compounds in human cancer cell lines: a comparative proteomic approach, Drug Metabol. Drug Interact. 28 (2013) 167–176, https://doi.org/10.1515/DMDI-2013-0015.
[37] S.K. Katiyar, A.M. Roy, M.S. Baliga, Silymarin induces apoptosis primarily through a p53-dependent pathway involving Bcl-2/Bax, cytochrome c release, and caspase activation, Mol. Cancer Ther. 4 (2005) 207–216 http://www.ncbi.nlm.nih.gov/pubmed/15713892 , Accessed date: 6 May 2019.
[38] A.S. Mendo, S. Figueiredo, C. Roma-Rodrigues, P.A. Videira, Z. Ma, M. Diniz, M. Larguinho, P.M. Costa, J.C. Lima, A.J.L. Pombeiro, P.V. Baptista, A.R. Fernandes, Characterization of antiproliferative potential and biological targets of a copper compound containing 4′-phenyl terpyridine, JBIC J. Biol. Inorg. Chem. 20 (2015) 935–948, https://doi.org/10.1007/s00775-015-1277-z.
[39] C. Slator, Z. Molphy, V. McKee, A. Kellett, Triggering autophagic cell death with a di-manganese(II) developmental therapeutic, Redox Biol. 12 (2017) 150–161, https://doi.org/10.1016/J.REDOX.2017.01.024.
[40] J. Van Limbergen, C. Stevens, E. Nimmo, D. Wilson, J. Satsangi, Autophagy: from basic science to clinical application, Mucosal Immunol. 2 (2009) 315–330, https://doi.org/10.1038/mi.2009.20.
[41] O.A. Lenis-Rojas, A.R. Fernandes, C. Roma-Rodrigues, P.V. Baptista, F. Marques, D. Pérez-Fernández, J. Guerra-Varela, L. Sánchez, D. Vázquez-García, M.L. Torres, A. Fernández, J.J. Fernández, Heteroleptic mononuclear compounds of ruthenium (ii): synthesis, structural analyses, in vitro antitumor activity and in vivo toxicity on zebrafish embryos, Dalton Trans. 45 (2016) 19127–19140, https://doi.org/10.1039/C6DT03591D.
[42] M. Sutradhar, T. Rajeshwari, Roy Barman, A.R. Fernandes, F. Paradinha, C. Roma-Rodrigues, M.F.C. Guedes da Silva, A.J.L. Pombeiro, Mixed ligand aroylhydrazone and N-donor heterocyclic Lewis base Cu(II) complexes as potential antiproliferative agents, J. Inorg. Biochem. 175 (2017) 267–275, https://doi.org/10.1016/J.JINORGBIO.2017.07.034.
[43] L. Eloy, A.-S. Jarrousse, M.-L. Teyssot, A. Gautier, L. Morel, C. Jolivalt, T. Cresteil, S. Roland, Anticancer activity of silver-N-heterocyclic carbene complexes: caspase-independent induction of apoptosis via mitochondrial apoptosis-inducing factor (AIF), ChemMedChem 7 (2012) 805–814, https://doi.org/10.1002/cmdc.201200055.
[44] M. Batsala, B. Chandu, B. Sakala, S. Nama, S. Domatoti, Inductively coupled plasma mass spectrometry (ICP-MS), Int J Res Pharm Chem. 2 (2012) 671–680 www.ijrpc.com , Accessed date: 6 May 2019.
[45] S.E. Gomes, D.M. Pereira, C. Roma-Rodrigues, A.R. Fernandes, P.M. Borralho, C.M.P. Rodrigues, Convergence of miR-143 overexpression, oxidative stress and cell death in HCT116 human colon cancer cells, PLoS One 13 (2018) e0191607, , https://doi.org/10.1371/journal.pone.0191607.
[46] C. Garrido, S. Gurbuxani, L. Ravagnan, G. Kroemer, Heat shock proteins: endogenous modulators of apoptotic cell death, Biochem. Biophys. Res. Commun. 286 (2001) 433–442, https://doi.org/10.1006/BBRC.2001.5427.
[47] A. Freund, F.L. Zhong, A.S. Venteicher, Z. Meng, T.D. Veenstra, J. Frydman, S.E. Artandi, Proteostatic control of telomerase function through TRiC-mediated folding of TCAB1, Cell 159 (2014) 1389–1403, https://doi.org/10.1016/J.CELL.2014.10.059.
[48] P. Rustin, G. Kroemer, Mitochondria and cancer, Ernst Schering Found. Symp. Proc. 4 (2013) 1–289.
[49] M.M. Derry, R.R. Somasagara, K. Raina, S. Kumar, J. Gomez, M. Patel, R. Agarwal, C. Agarwal, Target identification of grape seed extract in colorectal cancer using drug affinity responsive target stability (DARTS) technique: role of endoplasmic reticulum stress response proteins, Curr. Cancer Drug Targets 14 (2014) 323–336 https://www.ingentaconnect.com/content/ben/ccdt/2014/00000014/00000004/art00001 (accessed May 6, 2019).
[50] M. Matsushima, T. Takahashi, M. Ichinose, K. Miki, K. Kurokawa, K. Takahashi, Structural and immunological evidence for the identity of prolyl aminopeptidase with leucyl aminopeptidase, Biochem. Biophys. Res. Commun. 178 (1991) 1459–1464, https://doi.org/10.1016/0006-291X(91)91057-J.
[51] L. Ravagnan, S. Gurbuxani, S.A. Susin, C. Maisse, E. Daugas, N. Zamzami, T. Mak, M. Jäättelä, J.M. Penninger, C. Garrido, G. Kroemer, Heat-shock protein 70 antagonizes apoptosis-inducing factor, Nat. Cell Biol. 3 (2001) 839–843, https://doi.org/10.1038/ncb0901-839.
[52] L. Whitesell, N.U. Lin, HSP90 as a platform for the assembly of more effective cancer chemotherapy, Biochim. Biophys. Acta-Mol. Cell Res. 1823 (2012) 756–766, https://doi.org/10.1016/J.BBAMCR.2011.12.006.
[53] A. Paul, Y.A. Garcia, B. Zierer, C. Patwardhan, O. Gutierrez, Z. Hildenbrand, D.C. Harris, H.A. Balsiger, J.C. Sivils, J.L. Johnson, J. Buchner, A. Chadli, M.B. Cox, The cochaperone SGTA (small glutamine-rich tetratricopeptide repeat-containing protein alpha) demonstrates regulatory specificity for the androgen, glucocorticoid, and progesterone receptors, J. Biol. Chem. 289 (2014) 15297–15308, https://doi.org/10.1074/jbc.M113.535229.
[54] P. Madureira, D. Waisman, P.A. Madureira, D.M. Waisman, Annexin A2: the importance of being redox sensitive, Int. J. Mol. Sci. 14 (2013) 3568–3594, https://doi.org/10.3390/ijms14023568.
[55] C.-Y. Wang, C.-F. Lin, Annexin A2: its molecular regulation and cellular expression in cancer development, Dis. Markers 2014 (2014) 1–10, https://doi.org/10.1155/2014/308976.
[56] Y. Yao, X.-Y. Jia, H.-Y. Tian, Y.-X. Jiang, G.-J. Xu, Q.-J. Qian, F.-K. Zhao, Comparative proteomic analysis of colon cancer cells in response to Oxaliplatin treatment, Biochim. Biophys. Acta-Proteins Proteomics. 1794 (2009) 1433–1440, https://doi.org/10.1016/J.BBAPAP.2009.06.005.
[57] V.H. Bull, E.M. Fargestad, M. Strozynski, B. Thiede, Temporal proteome profiling of taxol-induced mitotic arrest and apoptosis, Electrophoresis 31 (2010) 1873–1885, https://doi.org/10.1002/elps.200900780.
[58] L. Zhang, Q. Ji, Z.-H. Ni, J. Sun, Prohibitin induces apoptosis in BGC823 gastric cancer cells through the mitochondrial pathway, Asian Pacific J. Cancer Prev. 13 (2012) 3803–3807, https://doi.org/10.7314/APJCP.2012.13.8.3803.
[59] B. Zhang, Y. Zhang, M.-C. Dagher, E. Shacter, Rho GDP dissociation inhibitor protects cancer cells against drug-induced apoptosis, Cancer Res. 65 (2005) 6054–6062, https://doi.org/10.1158/0008-5472.CAN-05-0175.
[60] K.L. Keene, A.R. Quinlan, X. Hou, I.M. Hall, J.C. Mychaleckyj, S. Onengut-Gumuscu, P. Concannon, Evidence for two independent associations with type 1 diabetes at the 12q13 locus, Genes Immun. 13 (2012) 66–70, https://doi.org/10.1038/gene.2011.56.
[61] Bruker, APEX2, Bruker AXS Inc., Madison, Wisconsin, USA, 2012 (n.d.).
[62] G.M. Sheldrick, SADABS. Program for Empirical Absorption Correction, University of Gottingen, Germany, 2000 (n.d.).
[63] A. Altomare, M.C. Burla, M. Camalli, G.L. Cascarano, C. Giacovazzo, A. Guagliardi, A.G.G. Moliterni, G. Polidori, R. Spagna, *SIR* 97: a new tool for crystal structure determination and refinement, J. Appl. Crystallogr. 32 (1999) 115–119, https://doi.org/10.1107/S0021889898007717.
[64] G.M. Sheldrick, IUCr, a short history of *SHELX*, Acta Crystallogr. Sect. A Found. Crystallogr. 64 (2008) 112–122, https://doi.org/10.1107/S0108767307043930.
[65] L.J. Farrugia, *WinGX* and *ORTEP for Windows* : an update, J. Appl. Crystallogr. 45 (2012) 849–854, https://doi.org/10.1107/S0021889812029111.
[66] L.R. Raposo, C. Roma-Rodrigues, J. Jesus, L.M.D.R.S. Martins, A.J. Pombeiro, P.V. Baptista, A.R. Fernandes, Targeting canine mammary tumours via gold nanoparticles functionalized with promising Co(II) and Zn(II) compounds, Vet. Comp. Oncol. 15 (2017) 1537–1542, https://doi.org/10.1111/vco.12298.